Transition form factors of the $N^*(1535)$ as a dynamically generated resonance

D. Jido,[1] M. Döring,[2] and E. Oset[3]

[1]*Yukawa Institute for Theoretical Physics, Kyoto University, Kyoto 606-8502, Japan*

[2]*Institut für Kernphysik, Forschungszentrum Jülich GmbH, D-52425 Jülich, Germany*

[3]*Departamento de Física Teórica and IFIC, Centro Mixto Universidad de Valencia-CSIC, Institutos de Investigación de Paterna, Aptdo. 22085, E-46071 Valencia, Spain*

(Received 30 November 2007; revised manuscript received 5 May 2008; published 11 June 2008)

We discuss how electromagnetic properties provide useful tests of the nature of resonances, and we study these properties for the $N^*(1535)$ that appears dynamically generated from the strong interaction of mesons and baryons. Within this coupled-channels chiral unitary approach, we evaluate the $A_{1/2}$ and $S_{1/2}$ helicity amplitudes as a function of Q^2 for the electromagnetic $N^*(1535) \to \gamma^* N$ transition. Within the same formalism we evaluate the cross section for the reactions $\gamma N \to \eta N$. We find a fair agreement for the absolute values of the transition amplitudes, as well as for the Q^2 dependence of the amplitudes, within theoretical and experimental uncertainties discussed in the article. The ratios obtained between the $S_{1/2}$ and $A_{1/2}$ for the neutron or proton states of the $N^*(1535)$ are in qualitative agreement with experiment and there is agreement on the signs. The same occurs for the ratio of cross sections for the η photoproduction on neutron and proton targets in the vicinity of the $N^*(1535)$ energy. The global results support the idea of this resonance as being dynamically generated, hence, largely built up from meson baryon components. However, the details of the model indicate that an admixture with a genuine quark state is also demanded that could help obtain a better agreement with experimental data.

DOI: 10.1103/PhysRevC.77.065207 PACS number(s): 14.20.Gk, 13.40.Gp, 12.39.Fe, 24.85.+p

I. INTRODUCTION

The traditional picture of baryons as being made from three constituent quarks [1] is giving rise, in some cases, to more complicated structures. One of the ideas that has gained strength in recent times is that low-lying resonances of $J^P = 1/2^-, 3/2^-$ seem to be well represented in terms of states that are generated by the meson-baryon interaction in $L = 0$; in the $1/2^-$ case from the interaction of the octet of mesons of the π with the octet of baryons of the p [2–9] and in the $3/2^-$ from the interaction of the same mesons with the decouplet of baryons of the $\Delta(1232)$ [10,11]. The $\Lambda(1405)$, which actually comes as two poles in chiral theories [6], with this two-pole structure supported by experiment [12], has been long thought of as a kind of meson baryon molecule of the $\bar{K}N$ and $\pi\Sigma$ states [13,14], a structure similar to that provided by the chiral approaches mentioned above. The $N^*(1535)$ is one more resonance that appears in the two octets and one singlet of dynamically generated resonances coming from the interaction of the octet of mesons of the π with the octet of baryons of the p [6]. In fact, it was noted in Ref. [15], before the systematics of Ref. [6] were established, that the interaction provided by chiral Lagrangians put as kernel of the Lippmann Schwinger equation generated this resonance, which also appears in other work along similar lines [16,17].

The $N^*(1535)$ plays an important role in all processes of η production because it couples very strongly to ηN. This feature is actually provided automatically by the chiral theories, one of the points of support for the nature of this resonance as being dynamically generated. A recent study of the model dependence of the properties of this resonance is seen in Ref. [18].

From the point of view of a dynamically generated resonance the $N^*(1535)$ leads to fair descriptions of the $\pi N \to \eta N$ and $\gamma N \to \eta N$ reactions [15,17,19] and produces reasonable numbers for the ηN scattering lengths [2,17]. Yet, it has been argued that one of the important tests of the nature of a resonance is its electromagnetic form factors. Indeed, a meson-baryon resonance should get the Q^2 dependence basically from the meson cloud (we take as usual $Q^2 = -k^2$ with k being the photon momentum). If this is a pion, this light particle has a fairly large extent in the wave function, as a consequence of which the form factor of the resonance should fall relatively fast compared to ordinary quark models that confine the quarks at smaller distances. This is also the case for the proton at small Q^2, due to its meson cloud, which stabilizes later on at larger values of Q^2 where the quark components take over, as shown in chiral quark models [20–22]. We shall see that something special happens for the $N^*(1535)$, but in any case this is a very stringent test, because the chiral theory provides the normalization and the Q^2 dependence for the different transition form factors without any free parameter, once the parameters used in πN scattering with its coupled channels are fixed to scattering data.

Radiative decays of resonances from the point of view of their dynamically generated nature have been addressed in Ref. [23] for the $\Lambda(1520)$, in Ref. [24] for the $\Delta(1700)$, and in Ref. [25] for the two $\Lambda(1405)$ states. It concerns the decay of the resonances into a baryon and a real photon. Some work with virtual photons from this point of view is done in [2,26] for the electroproduction of η in the vicinity of the $N^*(1535)$ resonance. Meanwhile, experimental analyses have succeeded in extracting the helicity transition form factors for $N^*(1535) \to N\gamma$ $A_{1/2}$ and $S_{1/2}$, for both $N = p, n$, in a relatively wide range of Q^2 values [27].

We evaluate these form factors from the point of view of the $N^*(1535)$ as a dynamically generated resonance. For that purpose we shall extend the formalism of Refs. [24,25] to

virtual photons. The new formalism requires changes from the real photon case, but it is rewarding because it provides much more information, replacing the helicity transition amplitudes by functions of Q^2 and adding the new $S_{1/2}$ transition form factor that plays a role only for virtual photons. Hence, there is far more information to test the predictions of the model.

From the quark model point of view there has also been much work done on these helicity form factors [28–36]. A comparison of their prediction with experiment plus a compilation of results from different experiments can be seen in Refs. [27,37,38]. There are appreciable differences from one quark model to another and relativistic effects seem to be important, particularly in the $S_{1/2}$ helicity transition form factor. It should be noted that some of the models, particularly those incorporating relativistic effects [31,33,35], produce a fair agreement with data, in particular a good description of the Q^2 dependence of the form factor.

In our approach, the quarks enter through the meson and baryon components of the resonance and the Q^2 dependence is tied to the meson and baryon form factors, which we take from experiment, plus the particular Q^2 dependence of the loop functions from the meson-baryon coupled channels that build up the resonance. Thus, the final Q^2 dependence is a nontrivial consequence of chiral dynamics, which provides the coupling of the resonance to open and closed channels, the Q^2 dependence of the different loops, and the form factors of the mesons and baryons, particularly the mesons, as we shall see.

The results that we obtain are in fair agreement with experiment for both charged states and for the two transition form factors, hence providing extra support for the nature of the $N^*(1535)$ as being largely made from the interaction of meson-baryon coupled channels.

Some deficiency in the Q^2 dependence at large Q^2 could be an indication of a mixture of the meson-baryon components with a genuine quark component, which is also indicated by particular details of the chiral approach that we shall mention below.

II. HELICITY AMPLITUDE

We consider the production reaction of the $N(1535)$ resonance ($J^p = 1/2^-$) by inelastic electron-nucleon scattering as shown in Fig. 1. The $N(1535)$ is created by exchange of a virtual photon carrying momentum k. The initial N and final N^* momenta and masses are denoted by (p_i, M_N) and (P, M_{N^*}), respectively. The energy-momentum conservation reads

$$P = p_i + k. \tag{1}$$

There are two independent amplitudes for the electrotransition from $J^P = 1/2^+$ to $1/2^-$, $A_{1/2}$ and $S_{1/2}$, which are defined in terms of the transition electric current J_μ by

$$A_{1/2} = \sqrt{\frac{2\pi\alpha}{q_R}}\frac{1}{e}\left\langle N^*, J_z = \frac{1}{2}\middle|\, \epsilon_\mu^{(+)} J^\mu \,\middle| N, S_z = -\frac{1}{2}\right\rangle \tag{2}$$

$$S_{1/2} = \sqrt{\frac{2\pi\alpha}{q_R}}\frac{1}{e}\frac{|\vec{k}|}{\sqrt{Q^2}}\left\langle N^*, J_z = \frac{1}{2}\middle|\, \epsilon_\mu^{(0)} J^\mu \,\middle| N, S_z = \frac{1}{2}\right\rangle \tag{3}$$

with the fine structure constant $\alpha = e^2/4\pi$, the energy equivalent to that of a real photon $q_R = (W^2 - M_N^2)/(2W)$ and the photon-nucleon center-of-mass (c.m.) energy $W \equiv \sqrt{P^2}$. The polarization vectors of the photon, ϵ_μ, are given by

$$\epsilon_\mu^{\pm} = \frac{1}{\sqrt{2}}(0, \mp 1, -i, 0) \tag{4}$$

$$\epsilon_\mu^{0} = \frac{1}{\sqrt{Q^2}}(k, 0, 0, -k^0), \tag{5}$$

with $Q^2 = -k^2$, where we take the c.m. momenta $\vec{k}$ and $\vec{p}_i$ along the z axis.

Let us discuss the general expression of the transition current J^μ in the relativistic formulation. First of all, we recall the equation of motion for the initial nucleon

$$(\not{p}_i - M_N)u_i(p_i) = 0, \tag{6}$$

where $u_i(p_i)$ is the Dirac spinor for the initial nucleon normalized by

$$u_N = \sqrt{\frac{E_i + M_N}{2M_N}}\begin{pmatrix} 1 \\ \frac{\vec{\sigma}\cdot\vec{p}_i}{E_i + M_N} \end{pmatrix}\chi. \tag{7}$$

For the final N^*, we assume the pole dominance, so that we again have

$$(\not{P} - M_{N^*})u_f(P) = 0, \tag{8}$$

where $u_f(P)$ is the N^* Dirac spinor and M_{N^*} denotes the real part of the N^* mass. In the calculations of the helicity amplitude, the M_{N^*} is chosen as the N^* energy in the final state, $W \simeq 1535$ MeV.

It follows that the terms involving the γ matrix in J_μ are only of the form $\gamma\cdot\epsilon$, because we can move $\not{p}_i$ and $\not{P}$ through $\gamma_\mu\gamma_\nu - \gamma_\nu\gamma_\mu = g_{\mu\nu}$ to either the left or right end in the amplitudes, and they can be replaced by the masses by means of Eqs. (6) and (8). The term involving $\not{k}$ can also be replaced by the momentum conservation $\not{k} = \not{P} - \not{p}_i$. Thus, Lorentz invariance and momentum conservation (1) require the transition current J^μ to be written, in general, by the following three Lorentz scalar amplitudes:

$$J^\mu = (\mathcal{M}_1\gamma^\mu + \mathcal{M}_2 P^\mu + \mathcal{M}_3 k^\mu)\gamma_5. \tag{9}$$

The gauge invariance $k\cdot J = 0$, tells us that there are only two independent amplitudes among these three amplitudes, $\mathcal{M}_i$, giving the following relation:

$$(M_{N^*} + M_N)\mathcal{M}_1 + k\cdot P\mathcal{M}_2 + k^2\mathcal{M}_3 = 0. \tag{10}$$

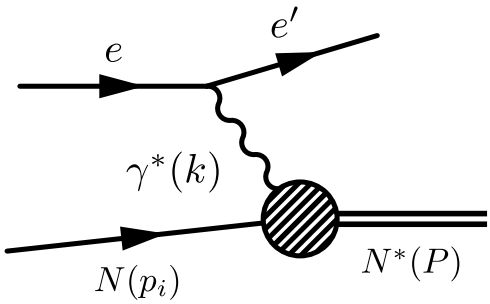

FIG. 1. Kinematics of the electroproduction of $N(1535)$.

Using the transition current (9), we evaluate the helicity amplitudes, $A_{1/2}$ and $S_{1/2}$, in the rest frame of the $N(1535)$ resonance. After some algebra, the helicity amplitudes are written in terms of the amplitude $\mathcal{M}_2$ and $\mathcal{M}_3$ by

$$A_{1/2} = \sqrt{\frac{2\pi\alpha}{q_R}}\sqrt{\frac{E_i+M_N}{2M_N}}\frac{1}{e}\frac{\sqrt{2}}{M_{N^*}+M_N}(k\cdot P\mathcal{M}_2 + k^2\mathcal{M}_3) \tag{11}$$

$$S_{1/2} = \sqrt{\frac{2\pi\alpha}{q_R}}\sqrt{\frac{E_i+M_N}{2M_N}}\frac{1}{e}\frac{-|\vec{k}|}{M_{N^*}+M_N} \times [M_{N^*}\mathcal{M}_2 + (M_{N^*}-M_N)\mathcal{M}_3]. \tag{12}$$

The transition current (9) can be written equivalently in the c.m. frame as

$$J^\mu = \sqrt{\frac{E_i+M_N}{2M_N}}\left\{\mathcal{M}_1\sigma^\mu + \left[\frac{\mathcal{M}_1}{(E_i+M_N)W} + \frac{\mathcal{M}_2}{E_i+M_N}\right]P^\mu\sigma\cdot k + \frac{\mathcal{M}_3}{E_i+M_N}k^\mu\sigma\cdot k\right\} \tag{13}$$

$$\equiv \mathcal{M}_1^{\rm NR}\sigma^\mu + \mathcal{M}_2^{\rm NR}P^\mu\sigma\cdot k + \mathcal{M}_3^{\rm NR}k^\mu\sigma\cdot k, \tag{14}$$

where $\sigma^\mu = (0,\vec{\sigma})$ and we take the c.m. frame $P^\mu = (W,\vec{0})$. Then the helicity amplitudes are written in terms of the amplitudes defined above, $\mathcal{M}_i^{\rm NR}$, as

$$A_{1/2} = \sqrt{\frac{2\pi\alpha}{q_R}}\frac{1}{e}\sqrt{2}\left(k\cdot P\mathcal{M}_2^{\rm NR} + k^2\mathcal{M}_3^{\rm NR}\right) \tag{15}$$

$$S_{1/2} = \sqrt{\frac{2\pi\alpha}{q_R}}\frac{-|\vec{k}|}{e}\left(W\mathcal{M}_2^{\rm NR} + k^0\mathcal{M}_3^{\rm NR}\right) \tag{16}$$

with the gauge invariance condition for the nonrelativistic amplitudes

$$\mathcal{M}_1^{\rm NR} + \mathcal{M}_2^{\rm NR}k\cdot P + \mathcal{M}_3^{\rm NR}k^2 = 0. \tag{17}$$

III. EVALUATION OF THE TRANSITION FORM FACTORS

A. Model of $N(1535)$ and photon coupling

In our approach, the $N(1535)$ resonance is dynamically generated in the s-wave meson-baryon scattering in the coupled channels of $\pi^- p, \pi^0 n, \eta n, K^+\Sigma^-, K^0\Sigma^0, K^0\Lambda$ for the neutron resonance (with neutral charge) and $\pi^0 p, \pi^+ n, \eta p, K^+\Sigma^0, K^0\Sigma^+, K^+\Lambda$ for the proton resonance (with +1 charge). The scattering amplitude for the $N(1535)$ resonance is described in Ref. [17] by means of the Bethe-Salpeter equation for meson-baryon scattering given by

$$T = V + VGT. \tag{18}$$

Based on the N/D method and the dispersion relation [5], this integral scattering equation can be reduced to a simple algebraic equation

$$T = (1 - VG)^{-1}V, \tag{19}$$

where the matrix V is the s-wave meson-baryon interaction given by the lowest order of the chiral perturbation theory, which is the Weinberg-Tomozawa interaction, given by

$$V_{ij} = -C_{ij}\frac{1}{4f^2}(2\sqrt{s} - M_i - M_j)\sqrt{\frac{M_i+E}{2M_i}}\sqrt{\frac{M_j+E'}{2M_j}}, \tag{20}$$

with the channel indices i, j, the baryon mass M, the meson mass m, the meson decay constant f, and the c.m. energy $\sqrt{s}$. The coefficient C_{ij} is the coupling strength of the meson and baryon, which is determined by the SU(3) group structure of the channel. The diagonal matrix G is the meson baryon loop function given in terms of the meson and baryon propagators by

$$G(\sqrt{s}) = i\int\frac{d^4q}{(2\pi)^4}\frac{M}{E(\vec{q})}\frac{1}{q^0 - E(\vec{q}) + i\epsilon} \times \frac{1}{(P-q)^2 - m^2 + i\epsilon} \tag{21}$$

with the total energy $P = (\sqrt{s},0,0,0)$ in the c.m. frame. For the baryon propagator we use the nonrelativistic form and neglect the negative energy propagation. The loop function should be regularized with proper schemes. In the practical calculation, we take dimensional regularization by using a covariant form of the positive energy part of the baryon propagator,

$$\frac{M}{E(\vec{q})}\frac{\Sigma_r u_r(\vec{q})\bar{u}_r(\vec{q})}{q^0 - E(\vec{q}) + i\epsilon} \simeq \frac{2M\,\Sigma_r u_r(\vec{q})\bar{u}_r(\vec{q})}{q^2 - M^2 + i\epsilon}. \tag{22}$$

In dimensional regularization, the loop function in each channel i is given by the following analytic expression:

$$\begin{aligned} G_i &= i\int\frac{d^4q}{(2\pi)^4}\frac{2M_i}{q^2 - M_i^2 + i\epsilon}\frac{1}{(P-q)^2 - m_i^2 + i\epsilon} \\ &= \frac{2M_i}{16\pi^2}\left\{a_i(\mu) + \ln\frac{M_i^2}{\mu^2} + \frac{m_i^2 - M_i^2 + s}{2s}\ln\frac{m_i^2}{M_i^2} \right. \\ &\quad + \frac{\bar{q}_i}{\sqrt{s}}\left[\ln\left(s - \left(M_i^2 - m_i^2\right) + 2\bar{q}_i\sqrt{s}\right)\right. \\ &\quad + \ln\left(s + \left(M_i^2 - m_i^2\right) + 2\bar{q}_i\sqrt{s}\right) \\ &\quad - \ln\left(-s + \left(M_i^2 - m_i^2\right) + 2\bar{q}_i\sqrt{s}\right) \\ &\quad \left.\left. - \ln\left(-s - \left(M_i^2 - m_i^2\right) + 2\bar{q}_i\sqrt{s}\right)\right]\right\}, \end{aligned} \tag{23}$$

where $\bar{q}_i$ is the three-momentum of the meson or baryon in the c.m. frame, μ is the scale of dimensional regularization, and $a_i(\mu)$ are subtraction constants, which are determined by a fit to the S_{11} and S_{31} partial waves of πN scattering [17]. Once these constants are fixed to the πN-scattering data, the amplitudes involving photons can be predicted without introducing any new free parameters.

It should be emphasized that the subtraction constants $a_i(\mu)$ are different for different channels i in the model of Ref. [17]. This is unlike the case of $\overline{K}N$ scattering and the $\Lambda(1405)$ resonance, where all the subtraction constants in the different channels are approximately equal and of natural size according

to Ref. [5]. The need for different subtraction constants in the case of πN scattering and the $N^*(1535)$ resonance has been interpreted recently [39] as a clear indication that the $N^*(1535)$ contains a mixture of a genuine quark state apart from the meson-baryon components. This conclusion has been reached by following an alternative method in which the subtraction constants have been chosen of natural order, and approximately equal, and a Castillejo-Dalitz-Dyson (CDD) pole is included that would give us an indication that extra components to the meson-baryon ones are needed in the $N^*(1535)$ wave function. The study of Ref. [39] clearly indicates that the effect of the CDD pole is negligible for the $\Lambda(1405)$ resonance but relevant for the the case of the $N^*(1535)$. We shall see that our approach, based on the meson baryon components exclusively, provides a fair description of data, but some remaining discrepancies indirectly hint to the need of extra components in the wave function.

The resulting amplitudes T^{ij} from Eq. (19) can be analytically continued to the complex plane of the scattering energy $s^{1/2}$. The amplitude has a pole in the complex plane that is identified with the resonance, and the coupling strengths g_i of the resonance to the meson-baryon channels is determined by the residues of the pole:

$$T^{ij}_{N^*}(\sqrt{s}) = \frac{g_i g_j}{\sqrt{s} - M_R + i\Gamma_R/2} + T^{ij}_{\rm BG}, \tag{24}$$

where $\sqrt{s}$ is the c.m. energy of the meson-baryon system and $T^{ij}_{\rm BG}$ is an amplitude for the nonresonant contributions. The pole positions of the resonance are obtained as

$$\sqrt{s} = 1537 - 37i\ ({\rm MeV}) \tag{25}$$

for the n^* (neutral charge) and

$$\sqrt{s} = 1532 - 37i\ ({\rm MeV}) \tag{26}$$

for the p^* (+1 charge). The values of the coupling constants are listed in Tables I and II. The coupling constants g_i characterize the structure of the N^*. The empirical evidence of larger coupling of the $N(1535)$ to ηN than that to πN is reproduced in this model. In addition, the couplings to the ΣK and ΛK channels are also large. This implies that the $N(1535)$ has large components of strangeness.

In the meson-baryon picture of the $N(1535)$ resonance, the photoproduction of the resonance from the nucleon is formulated through the photon couplings to the meson and baryon components of the $N^*(1535)$. Photon couplings and gauge invariance in the case of chiral unitary amplitudes are discussed in Refs. [40–42]. Here, we follow an approach similar to the one developed in Refs. [23–25] for real photons, extending it to virtual ones. Feynman diagrams to the transition form factors at one-loop level are shown in Fig. 2. In the loops,

TABLE I. Complex coupling constants g_i of n^* to the meson-baryon channels.

$\pi^- p$	$\pi^0 n$	ηn
$0.557 + 0.325i$	$-0.387 - 0.238i$	$-1.45 + 0.435i$
$K^+\Sigma^-$	$K^0\Sigma^0$	$K^0\Lambda$
$2.20 - 0.171i$	$-1.56 + 0.115i$	$1.39 - 0.0825i$

TABLE II. Coupling constants g_i of p^* to the meson-baryon channels.

$\pi^0 p$	$\pi^+ n$	ηp
$0.397 + 0.222i$	$0.555 + 0.322i$	$-1.47 + 0.432i$
$K^+\Sigma^0$	$K^0\Sigma^+$	$K^+\Lambda$
$1.56 - 0.133i$	$2.21 - 0.183i$	$1.37 - 0.100i$

all possible octet mesons and baryons contribute, namely $\pi^- p$, $\pi^0 n$, ηn, $K^+\Sigma^-$, $K^0\Sigma^0$, $K^0\Lambda$ for the neutron resonance (neutral charge) and $\pi^0 p$, $\pi^+ n$, ηp, $K^+\Sigma^0$, $K^0\Sigma^+$, $K^+\Lambda$ for the proton resonance (+1 charge). We sum all the contributions to the transition amplitudes. In Figs. 2(a) and 2(b), the photon attaches to the meson and baryon in the loop, respectively. Figure 2(c) shows the Kroll-Ruderman coupling that is the contact interaction of the photon, meson, and baryon. Figures 2(d) and 2(e) have to be taken into account to keep gauge invariance. It seems that these diagrams contain a forbidden transition from the $1/2^+$ state of the proton to the $1/2^-$ state of the $N(1535)$, but negative energy propagation of the intermediate baryons in these diagrams is possible, having the opposite parity to the positive energy propagation. The positive energy part in motion also mixes different parity states through the different partial waves.

We calculate the transition amplitudes both in a nonrelativistic and relativistic formulations. The momentum of the baryon is small enough to describe the transition amplitudes in a nonrelativistic formulation. In addition, as already mentioned, in the construction of the $N(1535)$ in the meson-baryon scattering [17], we have used the nonrelativistic formulation in the elementary vertex and the baryon propagators as seen in Eqs. (20) and (23). Therefore, to keep consistency of the calculation of the photon couplings with the construction of the N^* resonance, the nonrelativistic calculation is preferable. One should mention that the fact that one fits subtraction constants to data largely washes out relativistic effects from the use of Eqs. (21) or (23) in the G function in a fair range of energies around the fitted point. Nevertheless, it is somewhat complicated to prove gauge invariance in the nonrelativistic formalism, because we need to take into account all the possible diagrams, including negative energy contributions, which are referred to as Z diagrams. To avoid this complication, we will also perform the calculation of the amplitudes in relativistic formulation, in which the negative energy contributions are automatically counted without introducing the Z diagrams, and we shall show that the relativistic calculation is exactly gauge invariant. This guarantees that each term in

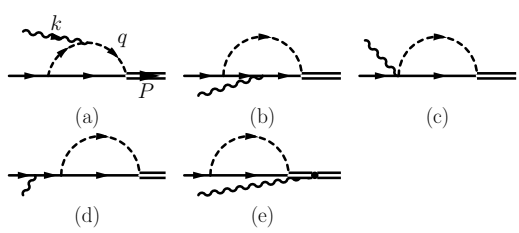

FIG. 2. Feynman diagrams for the transition form factor of $N(1535)$ at one loop level. The solid, dashed, wavy, and double lines denote octet baryons, mesons, photon, and $N(1535)$, respectively.

the $1/M$ expansion is gauge invariant. Exploiting this fact, in the nonrelativistic framework we calculate diagrams for leading amplitudes relying on gauge invariance and show that the next-to-leading terms are relatively small.

The basic interactions of the mesons and baryons are given by the following chiral Lagrangian:

$$\mathcal{L}_{MBB} = -\frac{D}{\sqrt{2}f}\,\mathrm{Tr}\,[\bar{B}\gamma_\mu\gamma_5\{\partial^\mu\Phi, B\}] - \frac{F}{\sqrt{2}f}\,\mathrm{Tr}\,[\bar{B}\gamma_\mu\gamma_5[\partial^\mu\Phi, B]] \tag{27}$$

with the meson and baryon fields, Φ and B, defined by

$$\Phi = \begin{pmatrix} \frac{1}{\sqrt{2}}\pi^0 + \frac{1}{\sqrt{6}}\eta & \pi^+ & K^+ \\ \pi^- & -\frac{1}{\sqrt{2}}\pi^0 + \frac{1}{\sqrt{6}}\eta & K^0 \\ K^- & \bar{K}^0 & -\frac{2}{\sqrt{6}}\eta \end{pmatrix} \tag{28}$$

$$B = \begin{pmatrix} \frac{1}{\sqrt{2}}\Sigma^0 + \frac{1}{\sqrt{6}}\Lambda & \Sigma^+ & p \\ \Sigma^- & -\frac{1}{\sqrt{2}}\Sigma^0 + \frac{1}{\sqrt{6}}\Lambda & n \\ \Xi^- & \Xi^0 & -\frac{2}{\sqrt{6}}\Lambda \end{pmatrix}. \tag{29}$$

The MBB couplings from these Lagrangian are given by $g_A^i/(2f)$ with the corresponding axial vector coupling g_A^i and the meson decay constant f. The axial vector couplings are given in terms of the D and F parameters in the Lagrangian (27) as listed in Table III. For the meson decay constant, we use $f = 93$ MeV for all channels in our calculation. The values of D and F for the axial vector couplings are taken from Ref. [43] as

$$D = 0.85 \pm 0.06, \quad F = 0.52 \pm 0.04. \tag{30}$$

These values are determined by the experimental data of the hyperon axial vector couplings, neglecting higher-order corrections. The photon couplings to mesons and baryons are given by the gauge couplings:

$$\mathcal{L}_{\gamma B} = -e\,\mathrm{Tr}\,[\bar{B}\gamma_\mu[Q_{\mathrm{ch}}, B]]A^\mu \tag{31}$$

$$\mathcal{L}_{\gamma M} = ie\,\mathrm{Tr}\,[\partial_\mu\Phi[Q_{\mathrm{ch}}, \Phi]]A^\mu, \tag{32}$$

with the charge matrix $Q_{\mathrm{ch}} = \mathrm{diag}(\frac{2}{3}, -\frac{1}{3}, -\frac{1}{3})$. The Kroll-Ruderman terms, the γMBB couplings, are obtained by replacing the derivative acting on the meson fields, $\partial_\mu\Phi$, with the covariant derivative $D_\mu\Phi = \partial_\mu\Phi + ieA_\mu[Q_{\mathrm{ch}}, \Phi]$ in the interaction Lagrangian (27) to realize the gauge invariance. The Kroll-Ruderman terms are proportional to the meson charge Q_M. For the couplings of the meson-baryon to the N^* resonance, we take a Lorentz scalar form representing the s-wave nature and the coupling strengths are taken from the chiral unitary approach as given in Tables I and II.

TABLE III. The axial vector coupling g_A^i for each channel. The values of D and F are given in Eq. (30).

Channel	$np\pi^-$	$nn\pi^0$	$nn\eta$
g_A^i	$\sqrt{2}(D+F)$	$-D-F$	$\frac{1}{\sqrt{3}}(-D+3F)$
	$n\Sigma^-K^+$	$n\Sigma^0K^0$	$n\Lambda K^0$
	$\sqrt{2}(D-F)$	$-D+F$	$-\frac{1}{\sqrt{3}}(D+3F)$
Channel	$pp\pi^0$	$pn\pi^-$	$pp\eta$
g_A^i	$D+F$	$\sqrt{2}(D+F)$	$\frac{1}{\sqrt{3}}(-D+3F)$
	$p\Sigma^0K^+$	$p\Sigma^+K^0$	$p\Lambda K^+$
	$D-F$	$\sqrt{2}(D-F)$	$-\frac{1}{\sqrt{3}}(D+3F)$

B. Nonrelativistic formulation

In the nonrelativistic formulation, the leading terms of the $1/M$ expansions are shown in Figs. 2(a) and 2(c). The diagram in 2(b) is found to be of next-to-leading order due to the $1/M$ factor in the γBB coupling. In the c.m. frame of the N^*, which we take for the nonrelativistic calculation, the diagram in 2(d) vanishes, because there is a direct transition of $1/2^+$ to $1/2^-$. Figure 2(e) shows some contribution in this frame, but it is also found to be of next-to-leading order, because the contribution to the diagram in 2(e) is confirmed to vanish in the large M limit. Indeed, if one neglects the kinetic energy term of the baryon propagators in the loop ($\vec{p}^2/2M$), the loop function vanishes. It also vanishes in the rest frame of the nucleon because it again involves a $1/2^+$-to-$1/2^-$ transition.

We will obtain each component of Figs. 2(a) and 2(c) in the decomposition in terms of the Lorentz structure given in Eq. (14). Because the helicity amplitudes can be expressed by the $\mathcal{M}_2^{\mathrm{NR}}$ and $\mathcal{M}_3^{\mathrm{NR}}$ in Eqs. (15) and (16), we will calculate only these two amplitudes. The amplitudes $\mathcal{M}_2^{\mathrm{NR}}$ and $\mathcal{M}_3^{\mathrm{NR}}$ remain finite even with one loop integration. In fact, $\mathcal{M}_1^{\mathrm{NR}}$ does have divergence in the loop calculation, which should cancel with divergences coming from the other diagrams thanks to gauge invariance. Here we do not confirm the cancellation of the divergences, because we later show the complete cancellation in the relativistic formulation.

The Feynman rules for the nonrelativistic couplings are summarized in Fig. 3. In the figure, ϵ^μ denotes the photon polarization, and σ is a Lorentz covariant form of the spin matrix, $\sigma^\mu = (0, \vec{\sigma})$. g_A^i stands for the axial vector coupling constants of the baryons to the corresponding meson. The values of g_A^i for each channel are given in Table III. $g_{N^*}^i$ is the coupling strength of the N^* to the meson-baryon channel i.

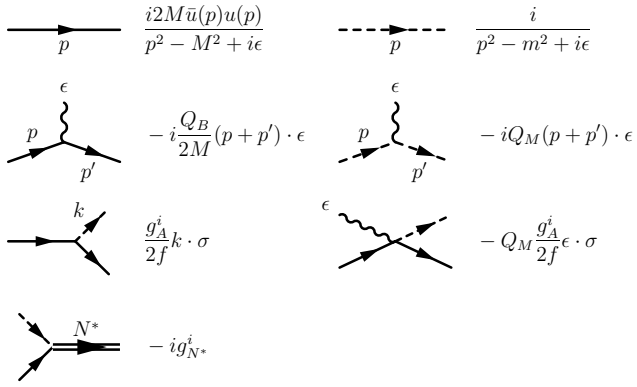

FIG. 3. Nonrelativistic Feynman rules for the propagator and the elementary vertices. The solid, dashed, wavy, and double lines denote octet baryons, mesons, photons, and $N(1535)$, respectively. M and m denote the baryon and meson masses, respectively. Q_B and Q_M are the charges of the baryon and meson.

The values of $g^i_{N^*}$ are listed in Table I and II. For the baryon propagator we use the covariant form from Eq. (22). The γBB coupling is used for the calculation of Fig. 2(b), which is not taken into account in our final result of the nonrelativistic calculation. But to confirm that subleading terms from the $1/M$ expansion are negligibly small, we have calculated the diagram in Fig. 2(b) using the nonrelativistic calculation. The γBB vertex is obtained by a nonrelativistic reduction of the interaction Lagrangian (31) as

$$-iQ_B\bar{u}\gamma\cdot\epsilon u \to -iQ_B\chi^\dagger\left[\epsilon^0-\frac{\vec{\epsilon}\cdot(\vec{p}+\vec{p}')}{2M}\right]\chi \tag{33}$$

$$\simeq -iQ_B\chi^\dagger\left[\frac{\epsilon\cdot(p+p')}{2M}\right]\chi, \tag{34}$$

where we have used the fact that the baryon kinetic energies are small in the nonrelativistic kinematics, $p^0\simeq p^{0\prime}\simeq M$, in the last expression. In Eqs. (33) and (34) we have neglected the magnetic term that behaves like $(\vec{\sigma}\times\vec{k})/2M$ that has one power less in the loop variable. In Sec. V B, we shall estimate the contributions from the convection current and the magnetic terms. In Eqs. (33) and (34), Q_B is the baryon charge such that it is e for the proton with $e^2/(4\pi)=\alpha\simeq 1/137$.

Let us start with Fig. 2(a). Applying the Feynman rules shown in Fig. 3, the amplitude $(-it=J\cdot\epsilon)$ for channel i is calculated as

$$\begin{aligned}-it^i_a &= \int\frac{d^4q}{(2\pi)^4}(-ig^i_{N^*})\frac{i2M_i}{(P-q)^2-M_i^2+i\epsilon}\left(\frac{g^i_A}{2f}\right)(q-k)\cdot\sigma\frac{i}{q^2-m_i^2+i\epsilon}(-iQ_M)(2q-k)\cdot\epsilon\frac{i}{(q-k)^2-m_i^2+i\epsilon}\\ &= iQ_MA_i\int\frac{d^4q}{(2\pi)^4}\frac{(q-k)\cdot\sigma(2q-k)\cdot\epsilon}{[(P-q)^2-M_i^2+i\epsilon](q^2-m_i^2+i\epsilon)[(q-k)^2-m_i^2+i\epsilon]},\end{aligned} \tag{35}$$

where the coefficient A_i is defined by

$$A_i=\frac{g^i_Ag^i_{N^*}M_i}{f}. \tag{36}$$

We use the Feynman parametrization of the integral

$$\frac{1}{abc}=2\int_0^1dx\int_0^xdy\frac{1}{[(a+(b-a)x+(c-b)y]^3}. \tag{37}$$

Then, using the integral variable q', such that $q=q'+P(1-x)+ky$ and renaming q' as q, we eliminate the linear terms of q in the denominator and obtain

$$-it^i_a=iQ_MA_i2\int_0^1dx\int_0^xdy\int\frac{d^4q}{(2\pi)^4}\frac{[q+(y-1)k]\cdot\sigma[2q+(2y-1)k+2(1-x)P]\cdot\epsilon}{\left(q^2-S^i_a+i\epsilon\right)^3}, \tag{38}$$

where we use $P\cdot\sigma=0$ in the c.m. frame and S^i_a is defined by

$$\begin{aligned}S^i_a &= 2P\cdot k(1-x)y-P^2x(1-x)-k^2y(1-y)\\ &\quad+M_i^2(1-x)+m_i^2x.\end{aligned} \tag{39}$$

In Eq. (38), even powers of q give contributions after performing the integration. The $q^\mu q^\nu$ term in the numerator that contributes to the $\mathcal{M}_1^{\rm NR}$ is divergent, whereas the terms with 0th power of q remain finite and contribute to the $\mathcal{M}_2^{\rm NR}$ and $\mathcal{M}_3^{\rm NR}$ amplitudes. Finally, after the integration, we obtain the $\mathcal{M}_2^{\rm NR}$ and $\mathcal{M}_3^{\rm NR}$ components for the channel i as

$$\mathcal{M}^{i({\rm NR})}_{2a}=\frac{Q_MA_i}{(4\pi)^2}\int_0^1dx\int_0^xdy\frac{2(y-1)(1-x)}{S^i_a-i\epsilon} \tag{40}$$

$$\mathcal{M}^{i({\rm NR})}_{3a}=\frac{Q_MA_i}{(4\pi)^2}\int_0^1dx\int_0^xdy\frac{(y-1)(2y-1)}{S^i_a-i\epsilon}, \tag{41}$$

where we have used

$$\int\frac{d^4q}{(2\pi)^4}\frac{1}{(q^2-S)^3}=-\frac{i}{(4\pi)^2}\frac{1}{2}\left(\frac{1}{S}\right). \tag{42}$$

In a similar way we evaluate the contribution from Fig. 2(b) that, as we mentioned, is of order $1/M$ of the previous ones and we obtain

$$\begin{aligned}\mathcal{M}^{i({\rm NR})}_{2b} &= -\frac{Q_BA_i}{(4\pi)^2}\int_0^1dx\int_0^xdy\frac{2y(1-x)}{S^i_b-i\epsilon}\\ \mathcal{M}^{i({\rm NR})}_{3b} &= -\frac{Q_BA_i}{(4\pi)^2}\int_0^1dx\int_0^xdy\frac{y(2y-1)}{S^i_b-i\epsilon}\end{aligned} \tag{43}$$

with

$$\begin{aligned}S^i_b &= 2P\cdot k(1-x)y-P^2x(1-x)-k^2y(1-y)\\ &\quad+m_i^2(1-x)+M_i^2x.\end{aligned} \tag{44}$$

For the Fig. 2(c), the amplitude has only the $\mathcal{M}_1^{\rm NR}$ component as seen in

$$
\begin{aligned}
-it_c^i &= \left(-ig_{N^*}^i\right)\int\frac{d^4q}{(2\pi)^4}\frac{i2M}{(P-q)^2-M^2+i\epsilon}\\
&\quad\times\left(-Q_M\frac{g_A^i}{2f}\right)\epsilon\cdot\sigma\frac{i}{q^2-m^2+i\epsilon}\\
&= iQ_MA_i\int\frac{d^4q}{(2\pi)^4}\\
&\quad\times\frac{\epsilon\cdot\sigma}{[(P-q)^2-M^2+i\epsilon](q^2-m^2+i\epsilon)}. \qquad (45)
\end{aligned}
$$

Hence we do not need to perform further calculation for this amplitude.

Finally, the helicity amplitudes in the nonrelativistic formulation are obtained by summing all the channels and substituting the amplitudes (40) and (41) in Eqs. (15) and (16).

C. Relativistic formulation

In this subsection, we calculate the transition amplitudes in relativistic formulation at the one-loop level. One of our purposes for the relativistic calculation is to confirm gauge invariance of our formulation. Without the $1/M$ expansion, which has been performed in the nonrelativistic calculation, all the diagrams shown in Fig. 2 should be calculated to make the amplitudes gauge invariant at the one-loop level. Each diagram has divergence from the loop integral. It will be found that the divergence appears only in the $\mathcal{M}_1$ term. After testing gauge invariance by summing up all the diagrams, the amplitudes should be finite without any regularization, because gauge invariance assures cancellation of the divergences coming from each diagram. To check this cancellation of the divergences, we calculate the $\mathcal{M}_1$ terms from all the diagrams. To isolate the divergent parts of the amplitudes, we exploit dimensional regularization, which respects gauge invariance. The calculations are done in d dimension, and then we expand d around $d=4$ in terms of ε given by $d=4-2\varepsilon$. We also calculate the finite $\mathcal{M}_2$ and $\mathcal{M}_3$ to obtain the helicity amplitudes in the relativistic formulation. We will find again that only Figs. 2(a) and 2(b) contribute to the $\mathcal{M}_1$ and $\mathcal{M}_2$ amplitudes.

Let us start with Fig. 2(a). Using the Feynman rules shown in Fig. 4, the amplitude of the diagram (a) for the channel i is given by

$$
\begin{aligned}
-iT_a^i &= \int\frac{d^dq}{(2\pi)^d}(-ig_i)i\frac{\not P-\not q+M_i}{(P-q)^2-M_i^2+i\epsilon}\left(\frac{g_A^i}{2f}\right)\\
&\quad\times(\not q-\not k)\gamma_5 i\frac{1}{(q-k)^2-m_i^2+i\epsilon}i\frac{1}{q^2-m_i^2+i\epsilon}\\
&\quad\times(-iQ_M)(2q-k)\cdot\epsilon\\
&= iQ_MB_i\int\frac{d^dq}{(2\pi)^d}\\
&\quad\times\frac{(\not P-\not q+M_i)(\not q-\not k)\gamma_5(2q-k)\cdot\epsilon}{\left[(P-q)^2-M_i^2\right]\left[(q-k)^2-m_i^2\right]\left(q^2-m_i^2\right)}, \qquad (46)
\end{aligned}
$$

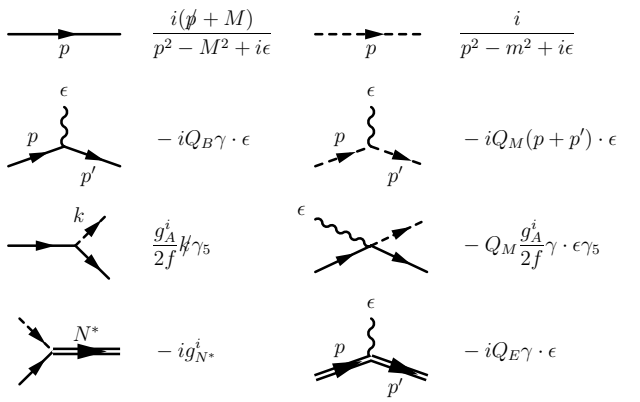

FIG. 4. Same as Fig. 3 for the relativistic formulation. Q_E stands for the external N^* charge.

where we define $B_i=(g_A^ig_{N^*}^i/2f)$. We can write expressions for all the other diagrams and then an explicit calculation shows that by substituting ϵ^μ by k^μ one obtains an exact cancellation of the terms, hence passing the ordinary test of gauge invariance. The coupling of the photon to all lines and vertices in the meson-baryon loop diagrams guarantees gauge invariance, as is commonly known [41,44].

We now come back to the amplitude T_a of Eq. (46) and, using the Feynman parameter integral (37), shifting the integral variable q to $q=q'+P(1-x)+ky$ and renaming q' by q, we find the integrand written as a function of q^2 as

$$
-iT_a^i = iQ_MB_i2\int_0^1dx\int_0^xdy\int\frac{d^dq}{(2\pi)^d}\frac{\frac{1}{2}q^2C_a+D_a}{\left(q^2-S_a^i+i\epsilon\right)^3}, \qquad (47)
$$

where S_a^i is defined in Eq. (39) and the coefficients C_a and D_a are defined in terms of the Lorentz components by

$$
\begin{aligned}
C_a &= C_{a1}\not\epsilon\gamma_5+C_{a2}P\cdot\epsilon\gamma_5+C_{a3}k\cdot\epsilon\gamma_5 \qquad (48)\\
D_a &= D_{a1}\not\epsilon\gamma_5+D_{a2}P\cdot\epsilon\gamma_5+D_{a3}k\cdot\epsilon\gamma_5. \qquad (49)
\end{aligned}
$$

After some algebra, noting that $g_\mu^\mu=d=4-2\varepsilon$ in the d-dimensional calculation, the coefficients C_{ai} and D_{ai} are found as

$$
\begin{aligned}
C_{a1}^i &= (M_N+M_i)\left(1+\frac{\varepsilon}{2}\right) \qquad (50)\\
C_{a2}^i &= 2(3x-2)+x\varepsilon \qquad (51)\\
C_{a3}^i &= 2(1-3y)-y\varepsilon \qquad (52)
\end{aligned}
$$

and

$$
\begin{aligned}
D_{a1}^i &= 0 \qquad (53)\\
D_{a2}^i &= 2(1-x)\big[(x-y)yk^2-x(x-y)M_{N^*}^2\\
&\quad+y(1-x)M_N^2+(y-1)M_iM_N\\
&\quad-(x-y)M_{N^*}(M_N+M_i)\big] \qquad (54)\\
D_{a3}^i &= (2y-1)\big[(x-y)yk^2-x(x-y)M_{N^*}^2\\
&\quad+y(1-x)M_N^2+(y-1)M_iM_N\\
&\quad-(x-y)M_{N^*}(M_N+M_i)\big]. \qquad (55)
\end{aligned}
$$

After the q integration, the divergent term is found only in the $\mathcal{M}_1$ amplitude as

$$\xi_a^i = -\frac{Q_M B_i}{(4\pi)^2}\frac{1}{\varepsilon}\frac{M_N + M_i}{2}\not{q}\gamma_5. \tag{56}$$

The divergent terms in the $\mathcal{M}_2$ and $\mathcal{M}_3$ vanish due to $\int_0^1 dx \int_0^x dy(3x-2) = 0$ and $\int_0^1 dx \int_0^x dy(1-3y) = 0$. To calculate the divergent term we have used the following formula:

$$\int \frac{d^d q}{(2\pi)^d}\frac{q^2}{(q^2 - S)^3} = \frac{i}{(4\pi)^{2-\epsilon}}\frac{4-2\epsilon}{2}\frac{\Gamma(\epsilon)}{\Gamma(3)}\left(\frac{1}{S}\right)^{\epsilon}$$
$$= \frac{i}{(4\pi)^2}\left[\frac{1}{\epsilon} - \log S - \frac{1}{2} - \gamma + \log 4\pi + \mathcal{O}(\epsilon)\right]. \tag{57}$$

The finite parts in the $\mathcal{M}_2$ and $\mathcal{M}_3$ terms are obtained as

$$\mathcal{M}_{2a}^i = \frac{Q_M B_i}{(4\pi)^2}\int_0^1 dx \int_0^x dy\left[2(3x-2)\log S_a^i - x + \frac{D_{a2}}{S_a^i}\right] \tag{58}$$

$$\mathcal{M}_{3a}^i = \frac{Q_M B_i}{(4\pi)^2}\int_0^1 dx \int_0^x dy\left[2(1-3y)\log S_a^i + y + \frac{D_{a3}}{S_a^i}\right], \tag{59}$$

where the first two terms in the integrands are from the finite parts of the divergent integrals and the last terms come from the finite integrals.

Next, let us move to the calculation of the Fig. 2(b). In a similar way, we obtain the finite $\mathcal{M}_2$ and $\mathcal{M}_3$ amplitudes as

$$\mathcal{M}_{2b}^i = \frac{Q_B B_i}{(4\pi)^2}\int_0^1 dx \int_0^x dy$$
$$\times\left[2(3y-1)\log S_b^i - y + 1 + \frac{D_{b3}}{S_b^i}\right] \tag{60}$$

$$\mathcal{M}_{3b}^i = \frac{Q_B B_i}{(4\pi)^2}\int_0^1 dx \int_0^x dy$$
$$\times\left[-2(3y-1)\log S_b^i + y - 1 + \frac{D_{b3}}{S_b^i}\right] \tag{61}$$

with S_b defined in Eq. (44) and

$$D_{b2}^i = 2[y(1-y)(x-y)k^2$$
$$- y(1-x)(x-y)M_{N^*}^2 - y^2(1-x)M_N^2 + xyM_N M_i$$
$$+ (x-y)(1-x)M_{N^*} + M_i)(M_N + M_i)] \tag{62}$$

$$D_{b3}^i = 2[-y(1-y)(x-y)k^2$$
$$+ y(1-x)(x-y)M_{N^*}^2 + y^2(1-x)M_N^2 - xyM_N M_i$$
$$+ y(x+y)(M_N + M_i)(M_{N^*} + M_N)]. \tag{63}$$

We have the divergent term in the $\mathcal{M}_1$ term as

$$\xi_b^i = -\frac{Q_B B_i}{(4\pi)^2}\frac{1}{\varepsilon}\frac{M_N - M_{N^*} - M_i}{2}\not{q}\gamma_5. \tag{64}$$

The amplitudes for Figs. 2(c), 2(d), and 2(e) have only the $\mathcal{M}_1$ components, which we do not use for the transition amplitudes; only the divergent terms are necessary for the present arguments. The divergent terms are found

$$\xi_c^i = \frac{Q_M B_i}{(4\pi)^2}\frac{1}{\varepsilon}\frac{M_{N^*} + 2M_i}{2}\not{q}\gamma_5 \tag{65}$$

$$\xi_d^i = -\frac{Q_E B_i}{(4\pi)^2}\frac{1}{\varepsilon}\frac{\left(M_{N^*}^2 - 2M_i^2 - 2m_i^2 + M_{N^*}M_i\right)}{2(M_N + M_{N^*})}\not{q}\gamma_5 \tag{66}$$

$$\xi_e^i = \frac{Q_E B_i}{(4\pi)^2}\frac{1}{\varepsilon}\frac{\left(M_N^2 - 2M_i^2 - 2m_i^2 - M_N M_i\right)}{2(M_{N^*} + M_N)}\not{q}\gamma_5. \tag{67}$$

At the end, collecting all the divergent terms of Figs. 2(a) to 2(e), we find that the divergent terms cancel according to

$$\sum_{A=a}^{e}\xi_A^i = -\left[\frac{B_i\not{q}\gamma_5}{(4\pi)^2}\right](Q_E - Q_B - Q_M)\frac{M_{N^*} - M_N + M_i}{2}\frac{1}{\varepsilon}$$
$$= 0, \tag{68}$$

due to the charge conservation $Q_E = Q_B + Q_M$. The cancellation takes place in each channel of the loop.

IV. RESULTS

In this section we show our results for the helicity amplitudes, $A_{1/2}$ and $S_{1/2}$, of the $N(1535)$ dynamically generated in meson-baryon scattering. In Fig. 5, we show our result for the $A_{1/2}$ amplitude of the proton resonance calculated in the nonrelativistic formulation [cf. Eqs. (15), (40), (41)] with the c.m. energy $W = 1535$ MeV. In the present calculation, we multiply the amplitudes obtained in the former section by the electromagnetic form factors of the mesons or baryons to which the photon couples. The form factors of the meson

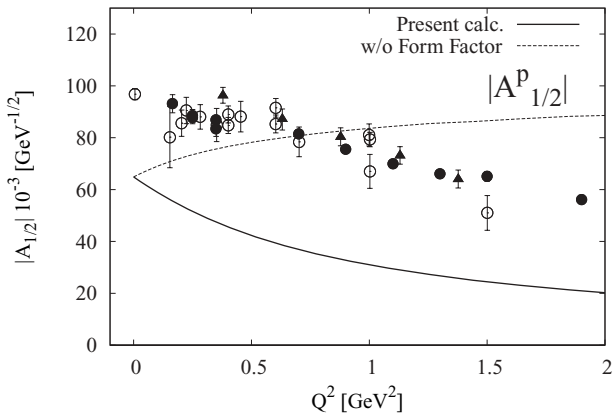

FIG. 5. Modulus of the $A_{1/2}$ helicity amplitude for the proton resonance as a function of Q^2 with $W = 1535$ MeV calculated in the nonrelativistic formulation. The solid (dotted) line shows the $A_{1/2}^p$ amplitude with (without) the form factor of the meson inside the loops given in Eq. (69). Marks with error bars are experimental data normalized by the N^* full width $\Gamma_{N^*} = 150$ MeV and the $N^* \to \eta N$ branching ratio $b_\eta = 0.55$. Filled triangles and circles are results of the CLAS collaboration taken from Refs. [37] and [45], respectively. Open circles show results of Refs. [46–49]. The values are taken from Ref. [46].

and baryons components of the resonance, together with the intrinsic Q^2 structure of the loops are responsible here for the Q^2 dependence of the helicity transition form factors. For the mesons and baryons form factors we take monolope form factors consistent with the values for the radii of the mesons. We take

$$F(Q^2) = \frac{\Lambda^2}{\Lambda^2 + Q^2} \tag{69}$$

with

$$\Lambda_\pi = 0.727\,(\text{GeV}) \tag{70}$$

$$\Lambda_K = 0.828\,(\text{GeV}), \tag{71}$$

which correspond to $\langle r^2 \rangle = 0.44$ fm^2 and $\langle r^2 \rangle = 0.34$ fm^2 for the pion and the kaon, respectively [50–52]. For the baryon form factor, we take the same form as for the corresponding meson to keep gauge invariance.

In Fig. 5, we show our result for the $A^p_{1/2}$ amplitude of the proton resonance calculated in the nonrelativistic formulation together with various experimental data. The c.m. energy is taken as $W = 1535$ MeV. Let us first discuss the Q^2 dependence of the helicity amplitude. The solid line denotes the modulus of the calculated amplitude multiplied by the meson form factor given in Eq. (69), whereas the dotted line shows the results without the meson form factor, which means that the Q^2 dependence comes only from the loop calculation performed in the previous section. In this case, the helicity amplitude increases as Q^2 increases. The inclusion of the form factors introduces a decreasing function of Q^2 that leads to a Q^2 dependence of the helicity amplitude in fair agreement with the experimental observation, although it falls faster than experiment because at $Q^2 = 0$ we need a renormalization factor of 1.45 to reach the data, whereas at $Q^2 = 1$ GeV^2 we need a factor of 2.15.

The absolute magnitude of our helicity amplitude looks underestimated if one compares our result directly with the experimental data shown in the figure. But it should be noted that extraction of the helicity amplitude from the experimental observables of the $\gamma p \to \eta p$ reaction is performed by using the following formula [45,46,53,54]:

$$A_{1/2}(Q^2) = \sqrt{\frac{W\Gamma_{N^*}}{2m_p b_\eta}\sigma(W, Q^2)}, \tag{72}$$

with a N^* full width Γ_{N^*}, a $N^* \to \eta N$ branching ratio b_η, a resonance part of the total cross section $\sigma(W, Q^2)$, the c.m. energy W, and the proton mass m_p. To obtain this relation, one assumes that the cross section is dominated by the single $N(1535)$ resonance and that the $S_{1/2}$ amplitude is small. For the experimental data shown in Fig. 5, the amplitudes are normalized by $\Gamma_{N^*} = 150$ MeV and $b_\eta = 0.55$ [45], which are obtained in a global fit of the cross section with the Breit-Wigner amplitude. However, the N^* width obtained in the present approach is $\Gamma_{N^*} \simeq 74$ MeV for the p^* as obtained from the pole position shown in Eq. (26), in which the half width is given by the imaginary part. The branching ratio b_η in this approach has been reported as $b_\eta \simeq 70\%$ [17]. This normalization difference would give us a factor 1.6 reduction

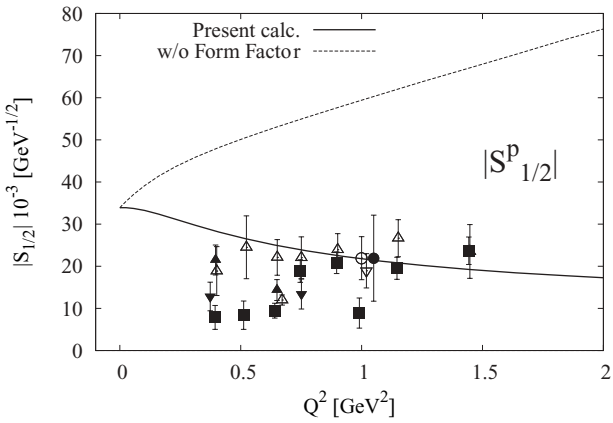

FIG. 6. Modulus of the $S_{1/2}$ helicity amplitude for the proton resonance as a function of Q^2 with $W = 1535$ MeV. The solid (dotted) line shows the $S^p_{1/2}$ amplitude with (without) the form factor of the meson inside the loops given in Eq. (69). The sign of this amplitude relative to $A^p_{1/2}$ is negative, both in experiment and theory. Solid triangles up (down) show the results from a combined analysis of π (η) electroproduction data [27,38]. The solid squares are from single-Q^2 fits from Ref. [55]. The empty triangles up are taken from Ref. [56]. The other data (empty circle and empty triangle down) are from Ref. [27].

in the normalization with respect to the data shown in Fig. 5. Similarly, should one use in the experimental analysis a $N(1535)$ width of the order of 90 MeV as found at BES [57] or the 100 MeV quoted in the last MAID2007 analysis [58], the results obtained would be in much better agreement with the theoretical results. We will come back to the discussion on the normalization later when discussing the photoproduction cross section in the present approach. Let us note that the value obtained here at $Q^2 = 0$ of $A^p_{1/2} = 64.88 \times 10^{-3}$ GeV$^{-1/2}$ is in excellent agreement with the most recent MAID2007 analysis reported in Ref. [58] of 66×10^{-3} GeV$^{-1/2}$.

The $S^p_{1/2}$ amplitude calculated in the nonrelativistic formulation is plotted in Fig. 6 together with experimental data. Although the modulus of $S_{1/2}$ is plotted in the figure, the ratio of $S_{1/2}$ to $A_{1/2}$ is nearly real and negative in agreement with experiment, where an implicit phase convention is taken that renders $A^p_{1/2}$ real and positive. Here we also show the effect of the meson form factor.

As mentioned before, Fig. 2(b), in which the photon couples to the baryon in the loop, gives subleading contributions in the $1/M$ expansion. This can be seen in Figs. 7, 8, 9, and 10. In these figures, the amplitudes with Fig. 2(a) only (solid line) are almost equivalent to those with both Figs. 2(a) and 2(b) (dashed line), and the contributions from Fig. 2(b) (dotted line) are smaller, in the present case, than typical corrections of 20–30% for the $1/M$ terms. Therefore, the helicity amplitudes in the nonrelativistic formulation around these energies are basically given by Fig. 2(a). We also plot the pion and kaon contributions separately. The figure shows that the pion contribution (dot-dashed line) is comparable with the kaon contribution (two-dotted line). This implies that the strange component is important in the structure of the $N(1535)$.

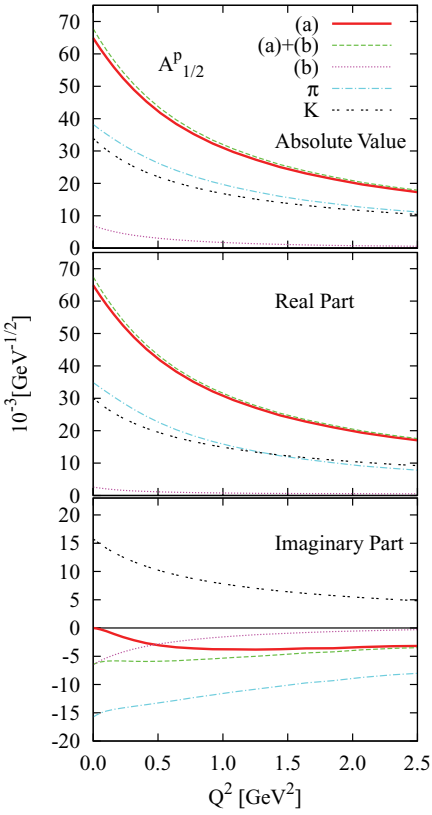

FIG. 7. (Color online) $A^p_{1/2}$ helicity amplitudes for the proton calculated in the nonrelativistic formulation as a function of Q^2. The upper, middle, and lower panels are, respectively, the modulus, real parts, and imaginary parts of the amplitudes. The phases of the amplitudes are set so that the $A^p_{1/2}$ amplitude has a real and positive value at $Q^2 = 0$. The solid lines show the calculation with Fig. 2(a) (meson pole term). The dashed and dotted lines stand for the calculations of sum of Figs. 2(a) and 2(b) and Fig. 2(b) only, respectively. The dot-dashed and two-dotted lines denote the pion and kaon contributions, respectively.

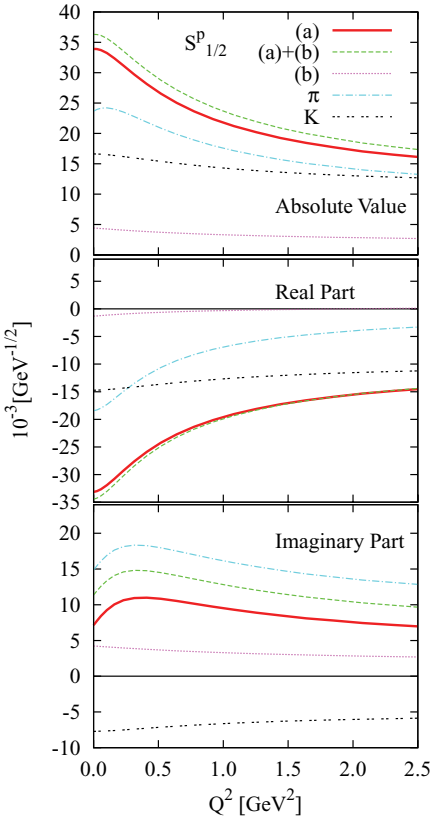

FIG. 8. (Color online) $S^p_{1/2}$ helicity amplitudes for the proton calculated in the nonrelativistic formulation as a function of Q^2. Same as described in the caption to Fig. 7.

Next, we report on results for the helicity amplitudes of the neutron. The n/p ratios of the helicity amplitudes, $A^n_{1/2}/A^p_{1/2}$ and $S^n_{1/2}/S^p_{1/2}$, are plotted in Fig. 11 as a function of Q^2. For a real photon at $Q^2 = 0$ we obtain the ratio $-0.79 + 0.11i$, which is almost a real value, and its modulus, 0.80. A multipole analysis [59] using the inclusive experimental data of Ref. [46] gives the negative sign value -0.84 ± 0.15 for $A^n_{1/2}/A^p_{1/2}$. Values of $|A^n_{1/2}|/|A^p_{1/2}|$ that are extracted from the ratio of the η photoproduction cross sections, σ_n/σ_p, are reported as 0.82 ± 0.04 in Ref. [60] and 0.819 ± 0.018 in Ref. [61]. The result obtained in our approach agrees with the experimental data in both sign and magnitude. This comparison is free from the normalization uncertainty of Eq. (72).

The values of the $A_{1/2}$ helicity amplitude at $Q^2 = 0$ are summarized in Table IV. The phases of the amplitudes are set so that the $A_{1/2}$ helicity amplitude for p^* has a real and positive value at $Q^2 = 0$. The ratios of the helicity amplitudes to that of p^* are also shown in the table. We also show the helicity amplitudes in the isospin decomposition:

$$A^{\rm IS}_{1/2} = \tfrac{1}{2}\left(A^p_{1/2} + A^n_{1/2}\right) \tag{73}$$

$$A^{\rm IV}_{1/2} = \tfrac{1}{2}\left(A^p_{1/2} - A^n_{1/2}\right). \tag{74}$$

In the nonrelativistic calculation we find that the value of the isoscalar component is much smaller than that of the isovector, which is consistent with experimental observation. The ratio of

TABLE IV. Values of the $A_{1/2}$ helicity amplitudes at $Q^2 = 0$ in units of $10^{-3}\text{GeV}^{-1/2}$ in the nonrelativistic (upper panel) and relativistic (lower panel) calculations. The ratios to the $A^p_{1/2}$ are also shown. The phases of the amplitudes are set so that the $A^p_{1/2}$ amplitude has a real and positive value at $Q^2 = 0$. IV and IS stand for isovector and isoscalar.

	$A_{1/2}$	$\lvert A_{1/2}\rvert$	$A_{1/2}/A^p_{1/2}$	$\lvert A_{1/2}/A^p_{1/2}\rvert$
	Nonrelativistic calculation			
p^*	64.88	64.88	–	–
n^*	$-51.54 + 7.21i$	52.04	$-0.79 + 0.11i$	0.80
IV	$58.21 - 3.61i$	58.32	$0.90 - 0.056i$	0.90
IS	$6.67 + 3.61i$	7.59	$0.10 + 0.056i$	0.12
	Relativistic calculation			
p^*	46.31	46.31	–	–
n^*	$-55.24 + 28.95i$	62.36	$-1.19 + 0.63i$	1.35
IV	$50.78 - 14.47i$	52.80	$1.10 - 0.31i$	1.14
IS	$-4.46 + 14.47i$	15.15	$-0.10 - 0.31i$	0.33

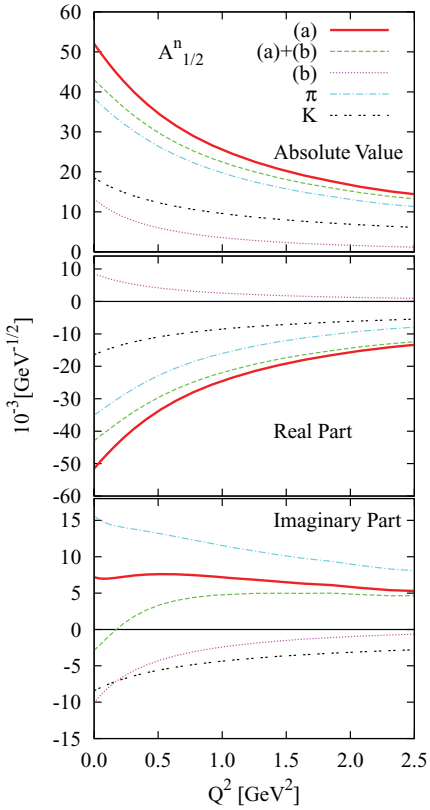

FIG. 9. (Color online) $A^n_{1/2}$ helicity amplitudes for the neutron calculated in the nonrelativistic formulation as a function of Q^2. The upper, middle, and lower panels are, respectively, the modules, real parts, and imaginary parts of the amplitudes. The phases of the amplitudes are set so that the $A^p_{1/2}$ amplitude has a real and positive value at $Q^2 = 0$. The solid shows the calculation with the Fig. 2(a) (meson pole term). The dashed and dotted lines stands for the calculations of sum of Figs. 2(a) and 2(b) and Fig. 2(b) only, respectively. The dot-dashed and two-dotted lines denote the pion and kaon contributions, respectively.

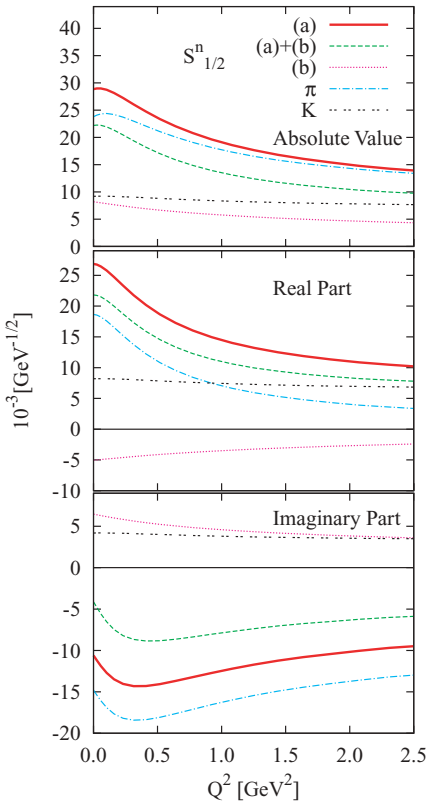

FIG. 10. (Color online) $S^n_{1/2}$ helicity amplitudes for the neutron calculated in the nonrelativistic formulation as a function of Q^2. Same as described in the caption to Fig. 9.

the isoscalar component to the p^* amplitude is $|A^{\rm IS}_{1/2}/A^p_{1/2}| = 0.12$ in our calculation, whereas in experiments it is found to be $A^{\rm IS}_{1/2}/A^p_{1/2} = 0.09 \pm 0.02$ in Ref. [60] and 0.09 ± 0.01 in Ref. [61].

It is also interesting to compare the values of our p^* and n^* helicity amplitudes $A_{1/2}$ at $Q^2 = 0$ with those of the PDG [62]. We obtain $0.065\ {\rm GeV}^{-1/2}$ and $-0.052\ {\rm GeV}^{-1/2}$ for the p^* and n^*, respectively, versus the values quoted in the PDG, which include uncertainties from the compilation of data of several analyses, $0.090 \pm 0.030\ {\rm GeV}^{-1/2}$ for the p^* and $-0.046 \pm 0.027\ {\rm GeV}^{-1/2}$ for the n^*. As one can see, the agreement, within uncertainties, is good.

V. DISCUSSION

A. Photoproduction of the η meson

In this section, we investigate the photoproduction of the η meson close to threshold energies to discuss the normalization of the helicity amplitude in the present approach. In the calculation of the helicity amplitude in Sec. III B, we have separated out the $N(1535)$ resonance contributions from the scattering amplitudes in which the $N(1535)$ is dynamically generated, by setting the c.m. energy as the resonance

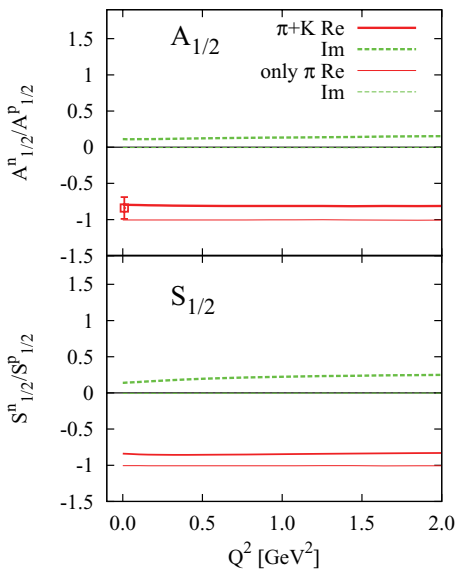

FIG. 11. (Color online) The n/p ratios of the helicity amplitudes with $W = 1535$ MeV. The upper and lower panels show the np ratios of the $A_{1/2}$ and $S_{1/2}$ amplitudes, respectively. The open square shows the value given in Ref. [59].

energy and multiplying the coupling strengths of the $N(1535)$ resonance to each channel, $g^i_{N^*}$, by the loop functions. For our purpose of calculating the η photoproduction cross section, we replace the coupling strengths, $g^i_{N^*}$, by the $MB \to \eta p$ scattering amplitudes, $t^{(i)}_{\eta p}$, obtained by the chiral unitary approach [17], where i denotes the initial meson baryon channel. The evaluation of these amplitudes is sketched here in Sec. III and done in detail in Ref. [17].

Following the above prescription for the η photoproduction amplitudes, we obtain the cross section of the photoproduction as

$$\sigma = \frac{M^2}{4\pi\, s}\,\frac{k_\eta}{k_\gamma}|t_{\gamma p\to\eta p}|^2, \tag{75}$$

where k_γ (k_η) is the photon (η) three-momentum in the c.m. frame and the T matrix is given by

$$|t_{\gamma p\to\eta p}|^2 = \frac{8m_p^2 + 8EE'}{16m_p^2}\left|\sum_{i=1}^{6}\mathcal{M}_1^{i(\mathrm{NR})}\frac{t^{(i)}_{\eta p}}{g^i_{N^*}}\right|^2, \tag{76}$$

where E (E') are the energies of the incoming (outgoing) proton in the c.m. frame. To obtain the $\mathcal{M}_1^{i(\mathrm{NR})}$ amplitude from the $\mathcal{M}_2^{i(\mathrm{NR})}$ and $\mathcal{M}_3^{i(\mathrm{NR})}$ amplitudes calculated in the previous section, we use the gauge invariance condition given in Eq. (17). Actually, the η photoproduction with a real photon has no contribution from the $\mathcal{M}_3^{i(\mathrm{NR})}$ amplitude, hence only one amplitude needs to be evaluated which we choose to be $\mathcal{M}_2$ that shows its finiteness immediately.

In Fig. 12, the total cross section of the present calculation (solid line) is plotted together with the data from Arndt [63] (dots). Our result of the η photoproduction cross section provides the right strength around the peak of the $N^*(1535)$ resonance but the width of the peak is narrower than the experiment as a result of the narrower widths of the $N(1535)$ resonance obtained by the present model.

In Fig. 13 we show the ratio of the cross sections of η photoproduction on the neutron over that on the proton, σ_n/σ_p, obtained in the nonrelativistic formulation, comparing our calculation with experimental data. The value of the ratio at $E_\gamma^{\mathrm{lab}} = 785$ MeV that corresponds to $E_{\mathrm{c.m.}} = 1535$ MeV

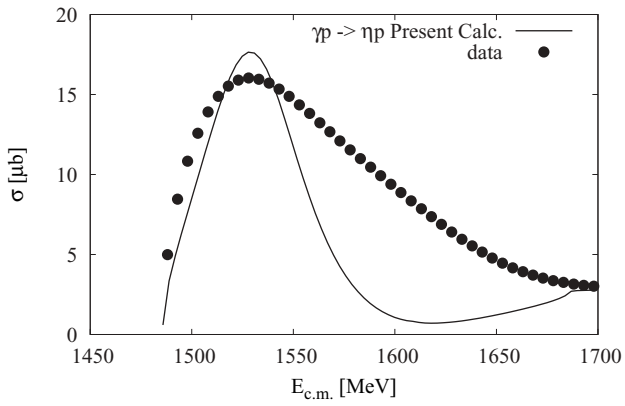

FIG. 12. Cross section for photoproduction of the η using the nonrelativistic formalism for the photon loop. Dots: Analysis from Arndt [63] (SAID database).

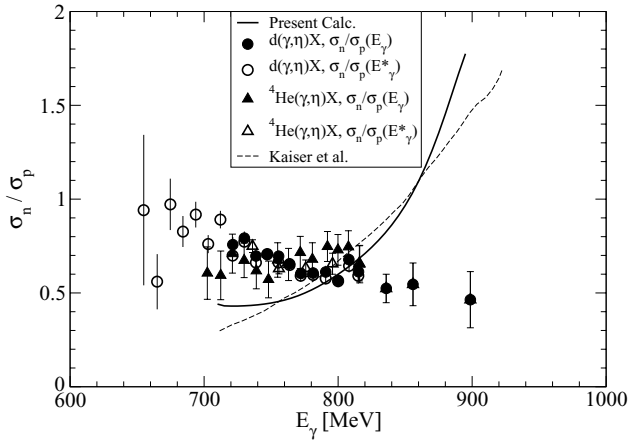

FIG. 13. Ratio of cross sections of photoproduction on the neutron over that on the proton, σ_n/σ_p, as a function of the photon energy E_γ in the laboratory frame. The data are taken from Ref. [61] for the deuteron target and Ref. [64] for the helium target. The dashed line is a theoretical calculation by Kaiser *et al*. in Ref. [2].

is found to be 0.53, which is quite consistent with the experimental data.

Although we are only concerned with the vicinity of the $N^*(1535)$ resonance, one cannot overlook the apparent discrepancy of the theory and experiment at photon energies above 800 MeV as shown in Fig. 13, which is also shared by the model of Ref. [2]. Only very recently have we obtained experimental information that brings a new perspective to these discrepancies. Indeed, in Ref. [65] the theoretical results of Fig. 13 are taken and folded with the Fermi motion of the nucleons in the deuteron to allow a realistic comparison with the experimental data. In Ref. [65] it is shown that the steep rise of the theoretical curve is softened to a curve in between the one of Fig. 13 and a horizontal line starting from 800 MeV. However, recent results from Ref. [66] for $\gamma n \to \eta n$ show a steady rise starting from $E_\gamma = 900$ MeV. These two facts together would render the apparent discrepancies into a rough qualitative agreement. Let us mention in this respect that the inclusion of the $\pi\pi N$ channel, although only qualitatively considered as shown in the next section, also works in the direction of softening the steep rise of Fig. 13. In any case, we must admit larger theoretical uncertainties at higher energies than around the resonance region, also including extra terms considered in Ref. [42] that would become relevant as one moves away from the resonance pole.

B. Higher-order couplings

In the nonrelativistic treatment of the photon loops from Fig. 2 in Sec. III B, the magnetic couplings of the photon to the baryons have been neglected as they are of higher order in the external photon momentum according to k/M. The convection part of the γBB coupling shows a similar p/M suppression, where p is a typical loop momentum. These higher-order terms have been neglected for the sake of consistency with the hadronic part of the model: as discussed after Eq. (21), only the positive energy part of the baryon propagator is taken

in the evaluation of the $MB \to MB$ scattering amplitude. In this section, the effects of the higher-order γBB coupling are studied, which can give an idea of theoretical uncertainties from these terms.

The photon-baryon coupling is given by

$$\mathcal{L}_{\gamma BB} = -\overline{\Psi}\left(Q_B \not{A} + \frac{\kappa e}{2M_N}\sigma^{\mu\nu}\partial_\mu A_\nu\right)\Psi, \qquad (77)$$

with $\sigma^{\mu\nu} = \frac{i}{2}[\gamma^\mu, \gamma^\nu]$, the baryon charge Q_B and the anomalous magnetic moment κ given in units of the nuclear magneton $\mu_N = e/(2M_N)$. In the nonrelativistic reduction of this interaction, only terms up to order $p/(2M)$ are considered that leads to the vertex

$$-it = \frac{i\,Q_B\,F(Q^2)}{2M}\,\vec{\epsilon}\,(\vec{p}+\vec{p}\,') + \frac{e\,G_M(Q^2)}{2M_N}\,\vec{\epsilon}\,(\vec{k}\times\vec{\sigma})\mu_B, \qquad (78)$$

where we have supplied the form factor $F(Q^2)$ given in Eq. (69) and the Sachs form factor $G_M(Q^2) = 1/(1 + Q^2/\Lambda_M^2)^2$, $\Lambda_M^2 = 0.71$ GeV^2 and μ_B is the baryon magnetic moments in units of μ_N from the PDG [62]. We use common form factors G_M for the Σ and Λ.

With the vertex from Eq. (78), the diagram in Fig. 2(b) can be calculated. For the convection part, the result has been already obtained in Eq. (43). The magnetic part of 2(b) is given by

$$t^{(i)}_{\rm mag} = -i\,e\,\mu_B^{(i)}\frac{g_A^i\,g_{N^*}^i}{2f}\,\vec{\epsilon}\,(\vec{\sigma}\times\vec{k})\int\frac{d^4q}{(2\pi)^4}\,\frac{\vec{\sigma}(\vec{P}-\vec{q})}{q^2-M_i^2} \times\frac{2M_i}{(q-k)^2-M_i^2}\,\frac{1}{(P-q)^2-m_i^2}. \qquad (79)$$

This expression is finite and not logarithmically divergent as the convection part of the γBB coupling or Figs. 2(a) and 2(c). The magnetic part is gauge invariant by itself as the structure of Eq. (79) shows. In Eq. (79), $m(M)$ are the masses of the meson (baryon) of channel (i), $P^2 \equiv s$, and $g^i_{N^*}$ are the coupling strengths to the $N(1535)$ from Tables I and II. For photoproduction, one obtains the amplitude $T(\gamma N \to \eta N)$ by replacing $g^i_{N^*}$ with the $MB \to N\eta\,T$ matrix as discussed in Sec. V A, summing over all channels i. The axial charges g^i_A are given in Table III. We also take into account the magnetic $\Sigma^0\Lambda$ transition. We choose a negative $\mu_{\Sigma^0\Lambda} = -1.61$ that is the prediction of the quark model [67], whereas only the modulus can be measured [62]. For the photon loops with a $\Sigma^0\Lambda$ transition, we use average masses for the baryons. For the unknown magnetic moment of the Σ^0, we take $\mu_{\Sigma^0} = \frac{1}{2}(\mu_{\Sigma^+} + \mu_{\Sigma^-}) = 0.65$ that is obtained by the SU(3) argument [68] and also consistent with the quark model.

Evaluating the loop integral using Feynman parameters we obtain

$$t^{(i)}_{\rm mag} = -ih^{(i)}(\vec{k}^2\vec{\sigma}\cdot\vec{\epsilon} - \vec{k}\cdot\vec{\sigma}\;\vec{k}\cdot\vec{\epsilon}) \qquad (80)$$

with

$$h^{(i)} = -e\mu_B^{(i)}\frac{g^i_{N^*}\,g^i_A\,M_i}{16\pi^2\,f}\int_0^1 dx\int_0^x dy\,\frac{y}{S_b^i - i\epsilon}. \qquad (81)$$

where S_b^i is defined in Eq. (44) and we used $P\cdot\sigma = 0$ in the c.m. frame. After summing all channels for the photon loop, we obtain the contribution to the helicity amplitudes from the magnetic couplings according to

$$A^{1/2}_{\rm mag} = -\sqrt{\frac{2\pi\alpha}{q_R}}\,\frac{\sqrt{2}\,\vec{k}^2}{e}\sum_{i=1}h^{(i)}. \qquad (82)$$

$$S^{1/2}_{\rm mag} = 0. \qquad (83)$$

The γBB coupling of Fig. 2(b) has a convection part and a magnetic part [cf. Eq. (78)], and both are of order $1/M$. Thus, we will treat both parts together and compare them to the previous results when only the leading-order couplings are considered. The latter appear in Figs. 2(a) and 2(c), whereas in the nonrelativistic calculations the diagrams in Figs. 2(d) and 2(e) do not contribute.

To see the effects of the various $1/M$ terms, we compared them in Table V. The phase is chosen in the way that $A^p_{1/2}(Q^2 = 0)$, including all $1/M$ terms, is real and positive.

TABLE V. The $1/M$ contributions from the baryon pole term for $A_{1/2}(Q^2 = 0)(10^{-3}\,\text{GeV}^{-1/2})$. See text for the different cases.

	$A^p_{1/2}$	$A^n_{1/2}$
I	$64.7 + 4i$	$-51.9 + 4i$
II	$67.7 - 2i$	$-42.7 - 5.5i$
III	$70.0 - 2.7i$	$-39.9 + 4.6i$
IV	74.7	$-44.5 + 1.9i$

Case (I) is from Figs. 2(a) and 2(c) only, without any γBB couplings. Case (II) also includes the convection part of the γBB coupling from Fig. 2(b). Case (III) additionally includes the magnetic part. Case (IV) includes, on top of the other contributions, the $\Sigma^0\Lambda$ transition magnetic part.

From the different contributions, we can see that the γBB coupling has moderate influence on the results: For $A^p_{1/2}$, the result increases due to the convection part and the magnetic part. For $A^n_{1/2}$, the various $1/M$ contributions lead to a decrease as Table V shows. As a result, the ratio $A^n_{1/2}/A^p_{1/2} = -0.60 + i\,0.03$ is smaller than the value of $-0.79 + i\,0.11$ found in the last section, where only the leading couplings were included.

In Fig. 14 the ratio of η photoproduction on the neutron over that on the proton is shown. The decrease, when including the higher-order couplings of Fig. 2(b), reflects the results from Table V that $A^p_{1/2}$ increases and $A^n_{1/2}$ decreases when including the $1/M$ corrections. In the same figure, we show the result when including additional ingredients for the rescattering model from Ref. [17] (dotted line). These are the $\pi\pi N$ channel in rescattering as well as a form factor for the $MB \to MB$ transitions. Coupling the photon to these ingredients is beyond the scope of this work; therefore, they are not included in the final results. Including these ingredients in the rescattering part, the ratio drops for higher photon energies, and this gives an idea of theoretical uncertainties coming from omitting the $\pi\pi N$ channel in the present study. For other observables discussed in this study, the additional ingredients from Ref. [17] lead only to very minor changes.

For consistency with the approach followed for meson-baryon scattering, the terms of order $1/M$ should be omitted,

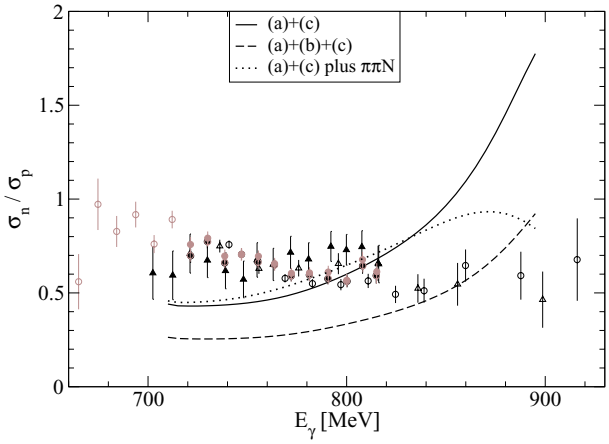

FIG. 14. (Color online) The ratio σ_n/σ_p including the baryon pole diagram (b) (dashed line), compared to the result without diagram (b) (solid line). Also, the result is shown when the $\pi\pi$N channel from [17] is included. The data is from Refs. [61,64] [see also Ref. [69]].

and the results of the former section should be used to compare with data. The discussion in this section gives us an idea of the uncertainties that one may have when considering the $1/M$ terms.

C. Result of the relativistic formulation

Here we briefly discuss our result for the $A^p_{1/2}$ amplitude of the p^* resonance calculated in the relativistic formulation given in Sec. III C. As already mentioned, the relativistic formulation is less consistent with the model of the $N(1535)$ resonance generated dynamically in the present approach than the nonrelativistic formulation. Therefore we rely on the nonrelativistic calculation. However, the Q^2 dependence could be given better by the relativistic calculation, particularly if we go to values of Q^2 of the order of 1 GeV^2 or above. On the other hand in the relativistic formulation we have found the cancellation of divergences coming from each diagram. In Fig. 15

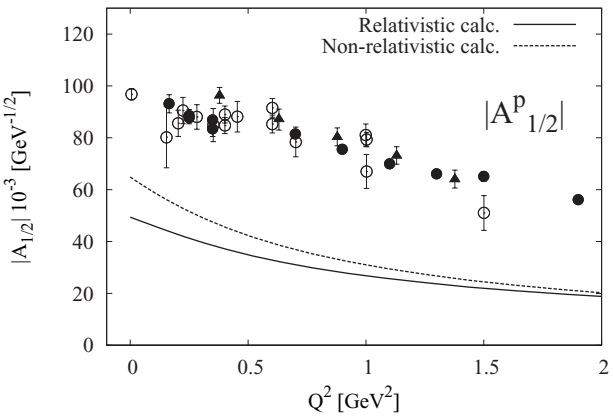

FIG. 15. Modulus of the $A_{1/2}$ helicity amplitude for the proton resonance as a function of Q^2 with $W = 1535$ MeV in relativistic formulation. The solid (dotted) line shows the $A^p_{1/2}$ amplitude calculated in the relativistic (nonrelativistic) formulation. The marks are the same as described in the caption to Fig. 5.

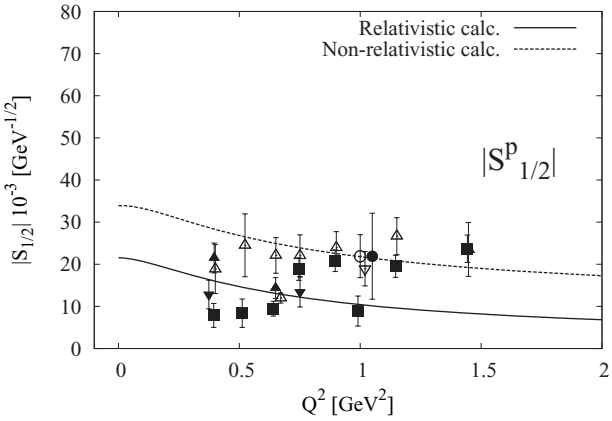

FIG. 16. Modulus of the $S_{1/2}$ helicity amplitude for the proton resonance as a function of Q^2 with $W = 1535$ MeV in relativistic formulation. The solid (dotted) line shows the $S^p_{1/2}$ amplitude calculated in the relativistic (nonrelativistic) formulation. The marks are the same as those described in the caption to Fig. 6.

we show the results for the $A^p_{1/2}$ amplitude in the relativistic calculation shown by the thick solid line in comparison with the nonrelativistic calculation shown by the dashed line. The relativistic result is a bit below the nonrelativistic calculation. We also plot the results for the $S^p_{1/2}$ amplitude obtained in the relativistic formulation in Fig. 16. The relativistic calculation gives a smaller result than the nonrelativistic one, as in the case of the $A^p_{1/2}$ amplitude, but the differences are now larger. This reflects the fact that the $S^p_{1/2}$ amplitude is more sensitive to small changes of the input and, consequently, one must accept larger theoretical uncertainties in this amplitude. The dispersion of the data seems to reflect a similar problem on the experimental side, the results proving also rather sensitive to the assumptions made in the different analyses.

Although we prefer the nonrelativistic results of $A^p_{1/2}$ at $Q^2 = 0$, as already mentioned, one can take this difference as a measure of the theoretical uncertainties. At $Q^2 = 0$ the relativistic result is some 25% below the nonrelativistic one. Taking into account 10% of uncertainty in the recent MAID2007 analysis [70] of $A^p_{1/2} = 66 \pm 7 \times 10^{-3}\text{GeV}^{-1/2}$, one finds good agreement of the theory with the MAID2007 results within uncertainties.

Let us note that in the relativistic calculation the factor needed to agree with data at $Q^2 = 0$ is 1.9 and at $Q^2 = 1$ GeV^2 the factor needed is 2.4. It indicates a faster fall down than experiment, 25% lower than experiment at $Q^2 = 1$ GeV^2 with a curve normalized at $Q^2 = 0$. This compares with 48% smaller strength than experiment at $Q^2 = 1$ GeV^2 of the nonrelativistic curve, normalized to the data at $Q^2 = 0$. This indicates that relativistic effects play some role at large Q^2, as one might think, along the line of similar findings in relativistic quark models [31,35].

We have also calculated the transition amplitudes using N^*BM couplings with a derivative of the type $\gamma_\mu\partial^\mu$ in the relativistic calculation. In this case, we have an extra momentum in the N^*BM coupling and this momentum is included in the loop integral. We also have an extra Kroll-Ruderman contact term. As a consequence, the cancellation

of the divergences is not complete in the case of $Q^2 > 0$, whereas, for the real photon, that is $Q^2 = 0$, the sum of the amplitudes is finite. From the viewpoint of consistency with the model of the N^*, one should not use the derivative coupling in the N^*BM vertex. In the unitarization based on the N/D method, we exploit the so-called elastic unitarity, in which the interactions V are evaluated on the mass shell. In the present case, the momenta in the Weinberg-Tomozawa couplings are set on the mass shell. Therefore, to maintain consistency with this procedure, the momentum in the N^*BM should have the value on the mass shell and should not be included in the loop integral. This means that a constant N^*BM coupling is more consistent with the present N^* model. In any case, just for illustrative purposes, the value that we obtain for $A^p_{1/2}$ with the off-shell derivative coupling is of the order of 90×10^{-3} GeV$^{-1/2}$. Our (preferred) nonrelativistic result lies between these two illustrative relativistic results.

VI. SUMMARY AND CRITICAL OBSERVATIONS

In this work we have addressed the evaluation of the electromagnetic helicity form factors for the electroproduction of the $N^*(1535)$ resonance considered as a dynamically generated resonance. For this purpose the coupling of the photon to the meson-baryon components of the $N(1535)$, previously studied within the chiral unitary approach to pion nucleon scattering, was considered. The calculations have been done relativistically and nonrelativistically, and both of them are found to lead to finite results for the transition amplitudes, as well as for η photoproduction that is evaluated simultaneously with the same formalism.

Our study finds interesting results that we summarize here. The amplitudes were obtained without any free parameters, because the couplings of the resonance to the channels have been obtained from a previous study of πN scattering. The agreement with the $A^p_{1/2}$ amplitude of the proton $N^*(1535)$ resonance is fair up to the normalization problem that we have discussed. Indeed, we showed that the absolute values of the experimental amplitudes were tied to assumptions on the total width of the resonance, which is still far from being a settled issue. We also showed that our results for $A_{1/2}$ at $Q^2 = 0$ are in perfect agreement with the most recent MAID2007 analysis of scattering and photoproduction data. The Q^2 dependence of the transition form factor obtained was in fair agreement with the experimental determination, although it provided a moderately faster fall down than experiment. This result is by no means obvious within the picture of a dynamically generated resonance, because the Q^2 dependence should be provided by the meson form factors and they fall much faster than these experimental form factors. Yet, we found that the theory, in the absence of the meson form factors, provided a rising function of Q^2, due to the structure of the loops involved, which led to a moderate decrease of the $N^*(1535)$ transition form factors when the meson form factors were considered.

The results obtained for the $S_{1/2}$ amplitude are also in fair agreement with those of experiment, both in size and the relative sign to the $A_{1/2}$ amplitude. It should be stressed that the nature of the loops, where some intermediate states can be put on shell, naturally leads to an imaginary part of the amplitude and hence one obtains complex transition form factors. Comparison with the data implies a choice of phase to make the $A_{1/2}$ amplitude real and with the sign chosen in the experimental analysis. However, once this is done, the rest of the amplitudes have very well-determined signs and phases. In this sense we found that the ratio of the $S_{1/2}$ to the $A_{1/2}$ amplitude was practically real and negative, and we also found that the ratio of the $A_{1/2}$ amplitude of the neutron resonance to that of the proton resonance was also practically real and of the order of -0.80, in good agreement with experiment.

It should be noted that the signs and strengths of the different amplitudes are a nontrivial consequence of the contribution of the different channels in the photon transition loops and of subtle interference of terms.

Thus we can say, that the agreement with the data is fair when it comes to the shape of the Q^2 dependence and good in the ratios of amplitudes that are free of the global normalization. All these features together provide a boost to the hypothesis of the $N^*(1535)$ as being a dynamically generated resonance. This of course does not exclude some other components beyond those of meson baryon exploited here, but the claim would be that these are the dominant components of the wave function and they show up clearly in the electromagnetic properties studied here. The slower experimental fall down with Q^2 could be an indication of the contribution of genuine quark components, along the lines of the work of Ref. [39] as we discussed in Sec. III A.

The discrepancies found in the normalization of $A^p_{1/2}$ for the proton deserve more attention. We have already commented that should one use the width of the $N^*(1535)$ of 90 MeV of BES, or 100 MeV of MAID2007, the experimental values would be lowered and the agreement between theoretical results and the experiment would be better. In fact, the agreement of the theoretical results for $A^p_{1/2}$ with the MAID2007 analysis is very good, as we have already noticed. But then we could look at the ratio $R = S^p_{1/2}/A^p_{1/2}$ and we find $R = 0.6$ at $Q^2 = 0.5\,\text{GeV}^2$. Experimentally, this ratio is $R \sim 0.2$ if we take an average value of $S_{1/2}$ over the different data, so the discrepancies in this ratio seem to be large. Certainly, the experimental ratio becomes much larger if we take the points with open triangles in Fig. 6 and then $R \sim 0.44$. This large dispersion of experimental values is understandable if one recalls that the contributions of the $S_{1/2}$ term in the $ep \to e'p\eta$ cross section (from where the data is extracted) is of the order of a few percent [27]. This, together with the experimental uncertainties in the normalization noted above, clearly indicate that large uncertainties in the experimental $S_{1/2}$ are indeed present. Further improvements in $S_{1/2}$ in the future will reveal if the discrepancies in the ratio R pointed out here are deficiencies of the model or stem from present experimental uncertainties or both. But it is clear that stronger claims in favor of the theoretical model are tied to a better precision in this experimental ratio, thus providing a justification for improved measurements of this magnitude.

At the same time we addressed the problem of η photoproduction on the proton and neutron with the same formalism. We found a cross section compatible with experiment in the $\gamma p \to \eta p$ reaction. This cross section also served to show

evidence that our approach misses strength of the reaction at energies beyond the $N^*(1535)$. This could be due to the fact that the width that we obtain for the resonance, of the order of $75 - 90$ MeV, is smaller than the experimental one or that the $\gamma p \to \eta p$ reaction collects strength from higher-energy resonances that are not dynamically generated and hence do not appear in our scheme. This issue is not settled in view of the large dispersion of results that one can find in the literature for the width of the $N^*(1535)$, from about 90 to 350 MeV. Furthermore, the ratio of the cross sections of $\gamma n \to \eta n$ to $\gamma p \to \eta p$ was obtained in fair agreement with experiment, particularly at energies close to the $N^*(1535)$.

Altogether, the information extracted in this article provides support for the idea of the $N^*(1535)$ resonance as being largely dynamically generated from the interaction of mesons and baryons, the dynamics of which seems to be well accounted for by chiral Lagrangians together with a proper coupled-channels unitary treatment of the interaction, as provided by the chiral unitary approach.

However, we also discussed that the recent study of Ref. [39] indicates the need for a genuine quark component of the $N^*(1535)$, which could provide strength at large Q^2 where our model, both in the nonrelativistic and relativistic versions, still provides a faster fall down with Q^2 than experiment.

ACKNOWLEDGMENTS

D.J. wishes to acknowledge the hospitality of the University of Valencia, where part of this work was done. This work is partly supported by DGICYT contract number FIS2006-03438, the Generalitat Valenciana, the collaboration agreement between the JSPS of Japan and the CSIC of Spain, the Grant for Scientific Research (numbers 18042001 and 20028004) and the Grant-in-Aid for the 21st Century COE "Center for Diversity and Universality in Physics" from the Ministry of Education, Culture, Sports, Science and Technology of Japan. This research is part of the EU Integrated Infrastructure Initiative Hadron Physics Project under contract number RII3-CT-2004-506078 and was done under Yukawa International Program for Quark-Hadron Sciences.

[1] N. Isgur and G. Karl, Phys. Rev. D **18**, 4187 (1978); S. Capstick and N. Isgur, *ibid*. **34**, 2809 (1986); L. Y. Glozman and D. O. Riska, Phys. Rep. **268**, 263 (1996); L. Y. Glozman, Z. Papp, and W. Plessas, Phys. Lett. **B381**, 311 (1996); see also the review by S. Capstick and W. Roberts, Prog. Part. Nucl. Phys. **45**, S241 (2000), and references therein.
[2] N. Kaiser, T. Waas, and W. Weise, Nucl. Phys. **A612**, 297 (1997).
[3] E. Oset and A. Ramos, Nucl. Phys. **A635**, 99 (1998).
[4] E. Oset, A. Ramos, and C. Bennhold, Phys. Lett. **B527**, 99 (2002); [Erratum-*ibid*. **B530**, 260 (2002)].
[5] J. A. Oller and U.-G. Meißner, Phys. Lett. **B500**, 263 (2001).
[6] D. Jido, J. A. Oller, E. Oset, A. Ramos, and U.-G. Meißner, Nucl. Phys. **A725**, 181 (2003).
[7] C. Garcia-Recio, J. Nieves, E. Ruiz Arriola, and M. J. Vicente Vacas, Phys. Rev. D **67**, 076009 (2003).
[8] C. Garcia-Recio, M. F. M. Lutz, and J. Nieves, Phys. Lett. **B582**, 49 (2004).
[9] T. Hyodo, S. I. Nam, D. Jido, and A. Hosaka, Phys. Rev. C **68**, 018201 (2003).
[10] E. E. Kolomeitsev and M. F. M. Lutz, Phys. Lett. **B585**, 243 (2004).
[11] S. Sarkar, E. Oset, and M. J. Vicente Vacas, Nucl. Phys. **A750**, 294 (2005); [Erratum-*ibid*. **A780**, 78 (2006)].
[12] V. K. Magas, E. Oset, and A. Ramos, Phys. Rev. Lett. **95**, 052301 (2005).
[13] R. H. Dalitz and S. F. Tuan, Phys. Rev. Lett. **2**, 425 (1959).
[14] R. H. Dalitz and S. F. Tuan, Ann. Phys. **10**, 307 (1960).
[15] N. Kaiser, P. B. Siegel, and W. Weise, Phys. Lett. **B362**, 23 (1995).
[16] J. Nieves and E. Ruiz Arriola, Phys. Rev. D **64**, 116008 (2001).
[17] T. Inoue, E. Oset, and M. J. Vicente Vacas, Phys. Rev. C **65**, 035204 (2002).
[18] A. Kiswandhi, S. Capstick, and S. Dytman, Phys. Rev. C **69**, 025205 (2004).
[19] M. Döring, E. Oset, and D. Strottman, Phys. Rev. C **73**, 045209 (2006).
[20] A. W. Thomas, S. Theberge, and G. A. Miller, Phys. Rev. D **24**, 216 (1981).
[21] E. Oset, R. Tegen, and W. Weise, Nucl. Phys. **A426**, 456 (1984); [Erratum-*ibid*. **A453**, 751 (1986)].
[22] V. E. Lyubovitskij, T. Gutsche, and A. Faessler, Phys. Rev. C **64**, 065203 (2001).
[23] M. Döring, E. Oset, and S. Sarkar, Phys. Rev. C **74**, 065204 (2006).
[24] M. Döring, Nucl. Phys. **A786**, 164 (2007).
[25] L. S. Geng, E. Oset, and M. Döring, Eur. Phys. J. A **32**, 201 (2007).
[26] B. Borasoy, E. Marco, and S. Wetzel, Phys. Rev. C **66**, 055208 (2002).
[27] V. D. Burkert and T. S. H. Lee, Int. J. Mod. Phys. E **13**, 1035 (2004).
[28] F. E. Close and Z. P. Li, Phys. Rev. D **42**, 2194 (1990).
[29] W. Konen and H. J. Weber, Phys. Rev. D **41**, 2201 (1990).
[30] M. Warns, H. Schroder, W. Pfeil, and H. Rollnik, Z. Phys. C **45**, 627 (1990).
[31] S. Capstick and B. D. Keister, Phys. Rev. D **51**, 3598 (1995).
[32] B. D. Keister, S. Capstick, *N* Physics*, edited by T.-S. H. Lee and W. Roberts (World Scientific, Singapore, 1997), p. 58.
[33] M. Aiello, M. M. Giannini, and E. Santopinto, J. Phys. G **24**, 753 (1998).
[34] E. Pace, G. Salme, and S. Simula, Few-Body Syst. Suppl. **10**, 407 (1999).
[35] D. Merten, U. Loring, K. Kretzschmar, B. Metsch, and H. R. Petry, Eur. Phys. J. A **14**, 477 (2002).
[36] M. M. Giannini, E. Santopinto, and A. Vassallo, Prog. Part. Nucl. Phys. **50**, 263 (2003).
[37] R. Thompson *et al*. (CLAS Collaboration), Phys. Rev. Lett. **86**, 1702 (2001).
[38] I. G. Aznauryan, V. D. Burkert, H. Egiyan, K. Joo, R. Minehart, and L. C. Smith, Phys. Rev. C **71**, 015201 (2005).
[39] T. Hyodo, D. Jido, and A. Hosaka, arXiv:0803.2550 [nucl-th].
[40] J. C. Nacher, E. Oset, H. Toki, and A. Ramos, Phys. Lett. **B461**, 299 (1999).

[41] B. Borasoy, P. C. Bruns, U.-G. Meißner, and R. Nißler, Phys. Rev. C **72**, 065201 (2005).
[42] B. Borasoy, P. C. Bruns, U.-G. Meißner, and R. Nißler, Eur. Phys. J. A **34**, 161 (2007).
[43] M. A. Luty and M. J. White, Phys. Lett. **B319**, 261 (1993).
[44] B. Julia-Diaz, T. S. H. Lee, T. Sato, and L. C. Smith, Phys. Rev. C **75**, 015205 (2007).
[45] H. Denizli *et al*. (CLAS Collaboration), Phys. Rev. C **76**, 015204 (2007).
[46] B. Krusche *et al*., Phys. Rev. Lett. **74**, 3736 (1995).
[47] F. W. Brasse *et al*., Nucl. Phys. **B139**, 37 (1978); F. W. Brasse *et al*., Z. Phys. C **22**, 33 (1984).
[48] U. Beck *et al*., Phys. Lett. **B51**, 103 (1974).
[49] H. Breuker *et al*., Phys. Lett. **B74**, 409 (1978).
[50] S. R. Amendolia *et al*. (NA7 Collaboration), Nucl. Phys. **B277**, 168 (1986).
[51] S. R. Amendolia *et al*., Phys. Lett. **B178**, 435 (1986).
[52] J. A. Oller, E. Oset, and J. E. Palomar, Phys. Rev. D **63**, 114009 (2001).
[53] T. G. Trippe *et al*. [Particle Data Group], Rev. Mod. Phys. **48**, S1 (1976); [Erratum-*ibid*. **48**, 497 (1976)].
[54] C. S. Armstrong *et al*. (Jefferson Lab E94014 Collaboration), Phys. Rev. D **60**, 052004 (1999).
[55] L. Tiator, D. Drechsel, S. Kamalov, M. M. Giannini, E. Santopinto, and A. Vassallo, Eur. Phys. J. A **19**, 55 (2004).
[56] L. Tiator and S. Kamalov, AIP Conf. Proc. **904**, 191 (2007).
[57] J. Z. Bai *et al*. (BES Collaboration), Phys. Lett. **B510**, 75 (2001).
[58] D. Drechsel, S. S. Kamalov, and L. Tiator, Eur. Phys. J. A **34**, 69 (2007).
[59] N. C. Mukhopadhyay, J. F. Zhang, and M. Benmerrouche, Phys. Lett. **B364**, 1 (1995).
[60] P. Hoffmann-Rothe *et al*., Phys. Rev. Lett. **78**, 4697 (1997).
[61] J. Weiss *et al*., Eur. Phys. J. A **16**, 275 (2003).
[62] W. M. Yao *et al*. (Particle Data Group), J. Phys. G **33**, 1 (2006).
[63] R. A. Arndt, W. J. Briscoe, I. I. Strakovsky, R. L. Workman, and M. M. Pavan, Phys. Rev. C **69**, 035213 (2004).
[64] V. Hejny *et al*., Eur. Phys. J. A **6**, 83 (1999).
[65] I. Jaegle, Ph.D. thesis, University of Basel, 2007 (private communication).
[66] I. Jaegle *et al*., arXiv:0804.4841[nucl-ex].
[67] T. M. Aliev, A. Ozpineci, and M. Savci, Phys. Lett. **B516**, 299 (2001).
[68] S. R. Coleman and S. L. Glashow, Phys. Rev. Lett. **6**, 423 (1961).
[69] B. Krusche and S. Schadmand, Prog. Part. Nucl. Phys. **51**, 399 (2003).
[70] L. Tiator (private communication).